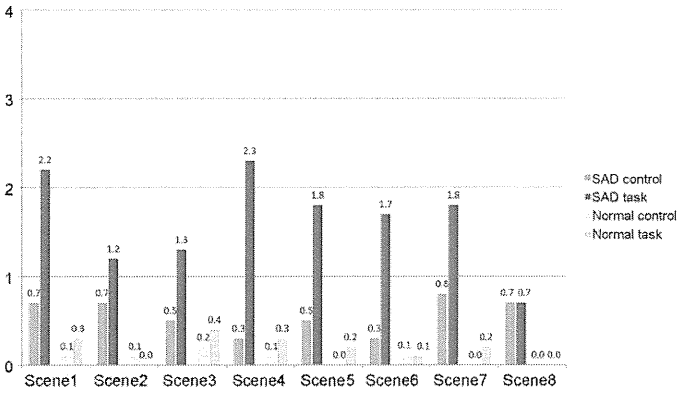

Fig. 1. Mean anxiety level of each scene. The patients with SAD showed higher total anxiety levels compared to the HC group during both the task conditions (SAD, 13.2 ± 5.7; HC, 1.7 ± 1.2, $F(1, 26) = 50.8$, $p < 0.001$, ANOVA) and the control conditions (SAD, 5.2 ± 3.5; HC, 0.7 ± 1.0, $F(1, 26) = 7.78$, $p < .01$, ANOVA). Concerning the difference of evoked anxiety among the eight scenes, the Scenes 1, 4, 5 and 7 showed significant higher anxiety than the Scene 8 in the task conditions. The Scenes 1 and 4 also showed higher anxiety than the Scene 2 ($F(7, 7) = 8.97$, $p < .01$, ANOVA).

symptoms with higher scores in the HDRS (SAD, 12.7 ± 9.4; HC, 0.7 ± 1.0, $p < .05$, Mann–Whitney U). They also showed higher anxiety scores in the STAI (trait: SAD, 62.2 ± 12.2; HC, 34.4 ± 10.4, $p < .01$, Mann–Whitney U; state: SAD, 53.2 ± 13.3; HC: 34.3 ± 8.5, $p < .05$, Mann–Whitney U). Three of the six patients were the generalized type, and the other three patients showed non-generalized symptoms during activities such as speaking or eating in public.

On the fMRI scans, the total anxiety levels during the task conditions were significant higher than the control conditions only in the SAD group (task 13.2 ± 5.7; control 5.2 ± 3.5, $F(1, 26) = 24.58$, $p < 0.001$, ANOVA) (Table 2). The patients with SAD showed higher total anxiety levels compared to the HC group during both the task conditions (SAD, 13.2 ± 5.7; HC, 1.7 ± 1.2, $F(1, 26) = 50.8$, $p < 0.001$, ANOVA), and the control conditions (SAD, 5.2 ± 3.5; HC, 0.7 ± 1.0, $F(1, 26) = 7.78$, $p < .01$, ANOVA). Concerning the difference of evoked anxiety among the eight scenes, the Scenes 1, 4, 5 and 7 showed significant higher anxiety than the Scene 8 in the task conditions. The Scenes 1 and 4 also showed higher anxiety than the Scene 2 ($F(7, 7) = 8.97$, $p < .01$, ANOVA) (Fig. 1).

The activated regions of each SAD and HC group are shown in Fig. 2 and Table 3. In the neuroimaging maps, the HC group showed greater common activation in the left posterior cingulate cortex (PCC), precuneus, bilateral cerebellum and right middle occipital and frontal gyrus ($p < 0.001$, uncorrected, random-effects model). Although the patients with SAD showed an activation pattern similar to that of the HC group, they showed significantly decreased activation compared to the HC group in the left cerebellum, left precuneus and PCC ($p < 0.001$, uncorrected, random-effects model, Fig. 3 and Table 4). The patients with SAD showed no areas of increased activation compared to the HCs.

4. Discussion

In the present study, we found increased activation in regions including PCC, precuneus, cerebellum, occipital and frontal gyrus on the fMRI trials using the social situation tasks. The patients with SAD showed decreased activation in the left cerebellum, precuneus, and PCC compared to the healthy controls. This study may be an essential fMRI study that examined the relationship between brain activities and social situations in patients with SAD.

We found characteristic activities in the PCC, precuneus, and cerebellum in patients with SAD compared to the healthy controls. The PCC and cuneus might play substantial roles in anxiety disorders. Several researchers using functional imaging methods reported decreased rCBF in the PCC in SAD (Warwick et al., 2008) and animal phobia (Fredrikson et al., 1995; Wik et al., 1993). In contrast, increased activation was shown in the PCC in SAD (Reiman, 1997) and PTSD (Bremner et al., 1999). Leibenluft et al. and his group found that the PCC and cuneus are more active during perception of socially relevant emotional stimuli, such as familiar faces (Gobbini et al., 2004; Leibenluft et al., 2004). In contrast, Gentili et al. (2009) reported that the PCC and precuneus had a lower reduction in activity in SAD compared to HC group by using fMRI during a stimulation task with emotional expressions on faces. They suggested that the PCC might play a substantial role in self-focused attention. In addition, functional imaging studies suggested that the precuneus involved in self-consciousness, such as reflective self-awareness, that involve rating ones own personality traits compared to those judged of other people. Gentili et al. (2009) also suggested that decreased activity in the PCC and precuneus might involve with impairments in default mode network (DMN), which play a pivotal role in social cognition. It is reasonable that activity of DMN might decrease during task condition compared to control condition. Concerning the deactivation in the PCC and precuneus with the patients, however, our results are not conclusive, because our design only included task and control conditions without a resting state as a baseline condition. It is reasonable to consider that the patients with SAD might already have been highly activated at the control condition and therefore they showed paradoxical decreased activation at the task condition compared to the healthy controls. Clark (Clark and Wells, 1995) suggested that self-focused attention in SAD increases access to negative thoughts and feelings. Patients

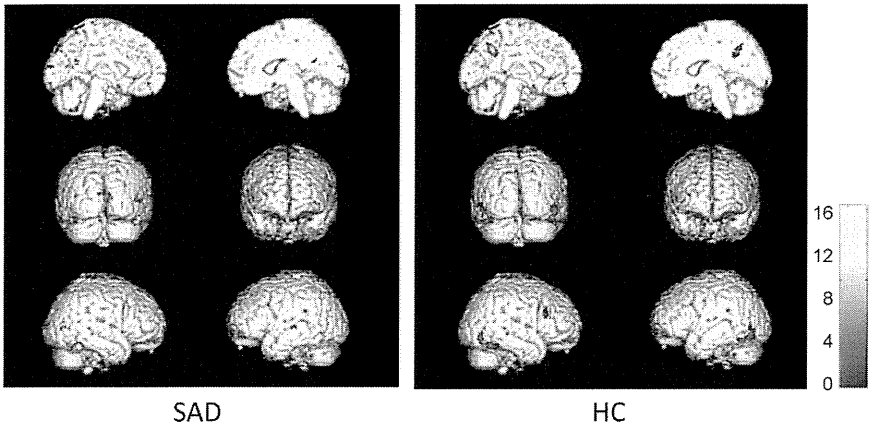

Fig. 2. Activated regions during task trials of the social situation task in SAD and HC group. In the neuroimaging maps, the HC group showed greater common activation in the left posterior cingulate cortex, precuneus, bilateral cerebellum and right middle occipital and frontal gyrus ($p < 0.001$, uncorrected).

Table 3
Activation maps of each SAD and HC groups during the task trial.

	Region	BA	Peak coordinate			T-value	Voxels
			x	y	z		
SAD	Right cerebellum	–	50	−50	−24	13.41	188
	Right cuneus	18	12	−98	8	15.69	41
	Right middle occipital gyrus	19	50	−72	8	9.15	25
	Left PCC	23	−6	−54	18	10.29	23
HC	Left PCC/precuneus	29/7	−4	−56	40	13.72	245
	Left cerebellum	–	−46	−62	−20	11.93	243
	Right cerebellum	–	50	−56	−20	11.77	113
	Right middle occipital gyrus	19	54	−70	−12	12.45	93
	Right middle frontal gyrus	46	42	22	22	9.19	51

Voxel-wise, significance thresholds of $p < 0.001$ (uncorrected) were used. BA: Brodmann's area, PCC: posterior cingulate cortex.

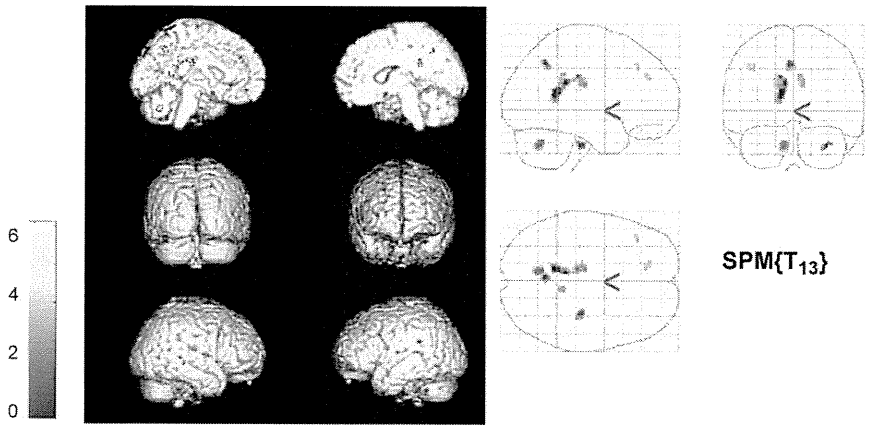

Fig. 3. Areas of greater activation in the HC group than in the SAD group. The patients with SAD showed significantly decreased activation compared to the HC group in the left cerebellum, left precuneus and bilateral PCC, though they showed an activation pattern similar to that of the HC group ($p < 0.001$, uncorrected).

Table 4
Areas of greater activation in HC group than in SAD group.

Region	BA	Peak coordinate			T-value	Voxels
		x	y	z		
Left PCC	29	−12	−48	18	5.86	107
Left PCC	29	−12	−26	32	5.10	71
Left cerebellum	–	−10	−64	34	5.05	50
Left precuneus	7	−4	−58	44	5.50	34
Right PCC	32	8	−44	24	4.48	30

Voxel-wise, significance thresholds of $p < 0.001$ (uncorrected) were used. BA: Brodmann's area, PCC: posterior cingulate cortex.

with SAD may have impairment in self-focused attention that may promote a distorted impression of themselves.

Recent neuroimaging studies have revealed the important role of the cerebellar cortex in higher neurocognitive functions such as cognition, attention, and memory. The cerebellum is enmeshed in the abundant prefrontal–subcortical–cerebellar connections, which have been suggested to play a role in coordinating complex mental and higher non-motor cognitive functions (Schmahmann and Pandya, 1997). Cerebellar activation is associated with various higher cognitive activities such as attention, executive control, language, working memory, emotion, and addiction (Strick et al., 2009). The cerebellum also may make a critical contribution to associative learning based on error feedback (Bellebaum and Daum, 2009). It may also play a substantial role in anxiety disorders. We found decreased activation in the cerebellum in patients with obsessive-compulsive disorder (OCD) while they performed the Stroop task during fMRI scanning compared to the healthy controls (Nakao et al., 2005a). We also found that they showed increased activation in the same region after symptom improvement due to effective treatment (Nakao et al., 2005b). Menzies et al. (2008) suggested that more widely distributed large-scale brain systems including posterior regions such as the cerebellum may be involved in anxiety disorders. The present study found evidence of a broad neuronal network dysfunction including the limbic system, parieto-posterior cortex, and cerebellum in SAD. At present, there are few studies that employed cognitive tasks other than perception of facial expressions as a stimulant task. Blair et al. (2008) reported that the patients with generalized SAD showed increased activation in the medial prefrontal cortex and bilateral amygdala compared to healthy volunteers while they are reading negative comments referring to themselves during fMRI.

On the other hand, previous neuroimaging studies mainly indicated increased activation of the amygdala and insular cortex in SAD. Tillfors et al. (2001) reported increased rCBF on PET scans in the right amygdala in patients with SAD during a public speaking task. They found, in contrast, decreased rCBF in the orbitofrontal complex and parietal, temporal, and insular cortices in patients with SAD compared to healthy controls. Their findings suggested that the amygdala may play an important role in emotion as a localized alarm center and that cortical structures might be involved in emotional evaluative processes. Stein et al. (2002) examined 15 patients with generalized SAD by fMRI while human facial stimuli were presented. The patients with SAD showed specific greater activation in the amygdala, uncus, and parahippocampus than healthy controls when viewing angry and contemptuous faces. They insisted that their findings of increased

left amygdala activation for certain face types contrasts is consistent with other studies that have used "unmasked" negatively valent faces as stimuli (Morris et al., 1998). Recently, Phan et al. (2006) examined 10 patients with SAD using fMRI. They found that activation of the amygdala in response to human faces displaying emotions such as disapproval and happiness correlated with the severity of the social anxiety symptoms. Thus, several neuroimaging studies reported abnormal activities in limbic regions such as the amygdala, hippocampus, and insular cortex. Etkin and Wager (2007) performed a meta-analysis of eight neuroimaging studies (Amir et al., 2005; Kilts et al., 2006; Lorberbaum et al., 2004; Phan et al., 2006; Stein et al., 2002; Straube et al., 2004, 2005; Tillfors et al., 2001) of SAD patients and found significant abnormal activities in the amygdala and insular cortex. Etkin & Wells compared regions-of-interest in anxiety disorders including SAD, specific phobia, and PTSD and suggested that hyperactivity in the amygdala and insular cortex was more common in SAD and specific phobia than in PTSD (Etkin and Wager, 2007).

We, however, did not find specific activation of these areas including the amygdala, insular cortex, and hippocampus in the present study. Regarding this negative findings, we should consider that the control scenes also might evoke social anxiety in the patients with SAD. Therefore, it is reasonable to consider that the patients might already have been highly activated at the control condition. Evoked emotion during the control condition might mask the activation of the amygdala and insular cortex during task condition. In addition, we should consider that some experimental scenes such as the Scenes 2 and 8 did not evoke sufficient anxiety to the patients. It might cause weakened activation of these regions.

The findings of the present study may contribute to previous neurocognitive findings that revealed abnormal activities of emotion-related regions including amygdala and insular cortex during facial perception in SAD. We, however, see several major limitations to the present study. An important limitation is the small number of subjects in each group, restricting the statistical power and enhancing the risk of type II errors. In the future, we will examine the brain mechanism in larger samples. Second, we did not find any abnormal activation in limbic areas such as the amygdala and insular cortex, although previous neuroimaging studies mainly indicated increased activation of these areas in SAD. Small sample size might be insufficient to conduct a reliable random-effects analysis within or between group analysis. Furthermore, our social situation tasks during fMRI scanning may be insufficient to reach the condition of fear, though the patients with SAD showed greater anxiety levels during scanning. Because we administered a common task including a combination of generalized and non-generalized types to all patients, some patients may have been essentially insensitive. In addition, the stimuli do not have enough ecological validity, as it has not been tested in other samples. We will redesign and test the task to make it more appropriate in further examinations. Furthermore, we did not consider the effects of the antidepressant drugs with which two patients were treated. Further study that employs larger samples and more appropriate procedures are needed.

5. Conclusion

In the present study, we found that the patients with SAD showed decreased activation in the left cerebellum, precuneus, and PCC compared to the healthy controls. In SAD, PCC might play a substantial role in self-focused attention and cerebellum might make a critical contribution to associative learning based on error feedback. This study may be an essential fMRI study that showed involvement of widely distributed large-scale brain systems including PCC and cerebellum while patients with SAD were exposed to social situations. The findings contribute to previous findings that revealed abnormal activities of emotion-related regions including the amygdala and insular cortex.

Acknowledgement

This study was supported by a Grant-in-Aid for Young Scientists (B) No. 18790836 from the Ministry of Education, Culture, Sports, Science and Technology.

Appendix A.

Attached files are the photographs displayed in the Social Situation Task during fMRI.

A.1. Task Scene 1

You are requested to express your opinion to seven company employees in the meeting.

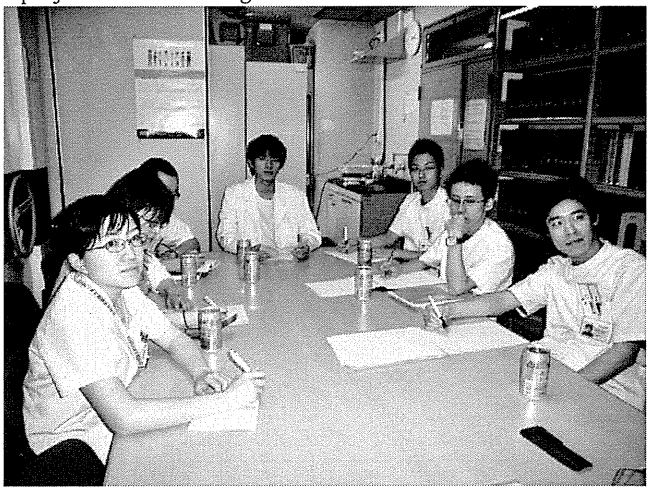

A.2. Task Scene 5

You have to sign your name in front of three female receptionists at the desk.

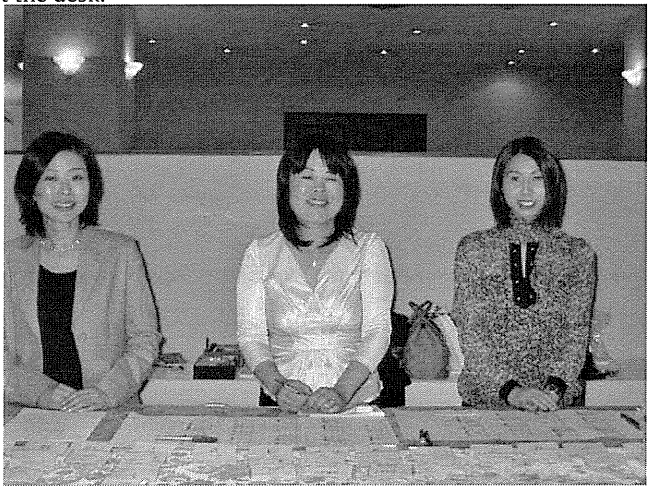

References

American Psychiatric Association, 1994. Diagnostic & Statistical Manual for Mental Disorders (DSM), 4th ed. American Psychiatric Press, Inc., Washington, DC.

Amir, N., Klumpp, H., Elias, J., Bedwell, J.S., Yanasak, N., Miller, L.S., 2005. Increased activation of the anterior cingulate cortex during processing of disgust faces in individuals with social phobia. Biological Psychiatry 57, 975–981.
Bellebaum, C., Daum, I., 2009. Mechanisms of cerebellar involvement in associative learning. Cortex (Epub ahead of print).
Blair, K., Geraci, M., Devido, J., Mccaffrey, D., Chen, G., Vythilingam, M., Ng, P., Hollon, N., Jones, M., Blair, R.J., Pine, D.S., 2008. Neural response to self- snd other referential praise and criticism in generalized social phobia. Archives of General Psychiatry 65, 1176–1184.
Bremner, J.D., Staib, L.H., Kaloupek, D., Southwick, S.M., Soufer, R., Charney, D.S., 1999. Neural correlates of exposure to traumatic pictures and sound in Vietnam combat veterans with and without posttraumatic stress disorder: a positron emission tomography study. Biological Psychiatry 45, 806–816.
Clark, D.M., Wells, A., 1995. A cognitive model of social phobia. In: Heiberg, R.G., Liebowitz, M.R., Hope, D. (Eds.), Social Phobia-diagnosis, Assessment and Treatment. Guiford, New York, pp. 69–93.
Etkin, A., Wager, T.D., 2007. Functional neuroimaging of anxiety: a meta-analysis of emotional processing in PTSD, social anxiety disorder, and specific phobia. American Journal of Psychiatry 164, 1476–1488.
First, M., Spitzer, R., Gibbon, M., Williams, J., 1996. Structured Clinical Interview for DSM-IV Axis I Disorders (Patient ed.). New York State Psychiatric Institute, New York.
Fredrikson, M., Wik, G., Annas, P., Ericson, K., Stone-Elander, S., 1995. Functional neuroanatomy of visually elicited simple phobic fear: additional data and theoretical analysis. Psychophysiology 32, 43–48.
Furmark, T., Tillfors, M., Marteinsdottir, I., Fischer, H., Pissiota, A., Långström, B., Fredrikson, M., 2002. Common changes in cerebral blood flow in patients with social phobia treated with citalopram or cognitive-behavioral therapy. Archives of General Psychiatry 59, 425–433.
Gentili, C., Ricciardi, E., Gobbini, M.I., Santarelli, M.F., Haxby, J.V., Pietrini, P., Guazzelli, M., 2009. Beyond amygdala: default mode network activity differs between patients with social phobia and healthy controls. Brain Research Bulletin 79, 409–413.
Gobbini, M.I., Leibenluft, E., Santiago, N., Haxby, J.V., 2004. Social and emotional attachment in the neural representation of faces. Neuroimage 22, 1628–1635.
Hamilton, M., 1960. A rating scale for depression. Journal of Neurology, Neurosurgery, and Psychiatry 23, 56–62.
Kessler, R.C., Chiu, W.T., Demler, O., Merikangas, K.R., Walters, E.E., 2005. Prevalence, severity, and comorbidity of 12-month DSM-IV disorders in the National Comorbidity Survey Replication. Archives of General Psychiatry 62, 617–627.
Kilts, C.D., Kelsey, J., Knight, B., Ely, T.D., Bowman, F.D., Gross, R.E., Selvig, A., Gordon, A., Newport, D.J., Nemeroff, C.B., 2006. The neural correlates of social anxiety disorder and response to pharmacotherapy. Neuropsychopharmacology 31, 2243–2253.
Leibenluft, E., Gobbini, M.I., Harrison, T., Haxby, J., 2004. Mothers' neural activation in response to pictures of their children and other children. Biological Psychiatry 56, 225–232.
Liebowitz, M., 1987. Social phobia. Modern Problems of Pharmacopsychiatry 22, 141–173.
Lorberbaum, J.P., Kose, S., Johnson, M.R., Arana, G.W., Sullivan, L.K., Hamner, M.B., Ballenger, J.C., Lydiard, R.B., Brodrick, P.S., Bohning, D.E., George, M.s., 2004. Neural correlates of speech anticipatory anxiety in generalized social phobia. Neuroreport 22, 2701–2705.
Menzies, L., Chamberlain, S.R., Laird, A.R., Thelen, S.M., Sahakian, B.J., Bullmore, E.T., 2008. Integrating evidence from neuroimaging and neuropsychological studies of obsessive-compulsive disorder: the orbitofronto-striatal model revisited. Neuroscience and Biobehavioral Reviews 32, 525–549.
Morris, J.S., Ohman, A., Dolan, R.J., 1998. Conscious and unconscious emotional learning in the human amygdala. Nature 393, 467–470.
Nakao, T., Nakagawa, A., Yoshiura, T., Nakatani, E., Nabeyama, M., Yoshizato, C., Kudoh, A., Tada, K., Yoshioka, K., Kawamoto, M., 2005a. A functional MRI comparison of patients with obsessive-compulsive disorder and normal controls during a Chinese character Stroop task. Psychiatry Research Neuroimaging 139, 101–114.
Nakao, T., Nakagawa, A., Yoshiura, T., Nakatani, E., Nabeyama, M., Yoshizato, C., Kudoh, A., Tada, K., Yoshioka, K., Kawamoto, M., Togao, O., Kanba, S., 2005b. Brain activation of patients with obsessive-compulsive disorder during neuropsychological and symptom provocation tasks before and after symptom improvement: a functional MRI study. Biological Psychiatry 57, 901–910.
Oldfield, R.C., 1971. The assessment and analysis of handedness: the Edinburgh inventory. Neuropsychologia 9, 97–113.
Phan, K.L., Fitzgerald, D.A., Nathan, P.J., Tancer, M.E., 2006. Association between amygdala hyperactivity to harsh faces and severity of social anxiety in generalized social phobia. Biological Psychiatry 59, 424–429.
Reiman, E., 1997. The application of positron emission tomography to the study of normal and pathologic emotions. The Journal of Clinical Psychiatry 58 (Suppl. 16), 4–12.
Schmahmann, J.D., Pandya, D.N., 1997. The cerebrocerebellar system. International Review of Neurobiology 41, 31–60.
Spielberger, C.D., Gourshi, R., Lushene, R., 1970. Manual for the State-Trait Anxiety Inventory. Consulting Psychologist Press, Palo Alto.
Stein, M.B., Chartier, M.J., Hazen, A.L., Kozak, M.V., Tancer, M.E., Lander, S., Furer, P., Chubaty, D., Walker, J.r., 1998. A direct-interview family study of generalized social phobia. American Journal of Psychiatry 155, 90–97.
Stein, M.B., Chartier, M.J., Lizak, M.V., Jang, K.L., 2001. Familial aggregation of anxiety-related quantitative traits in generalized social phobia: clues to understanding "disorder" heritability? American Journal of Medical Genetics 105, 79–83.
Stein, M.B., Goldin, P.R., Sareen, J., Zorrilla, L.T., 2002. Brown GG. Increased amygdala activation to angry and contemptuous faces in generalized social phobia. Archives of General Psychiatry 59, 1027–1034.
Straube, T., Kolassa, I.T., Glauer, M., Mentzel, H.J., Miltner, W.H., 2004. Effect of task conditions on brain responses to threatening faces in social phobics: an event-related functional magnetic resonance imaging study. Biological Psychiatry 56, 921–930.
Straube, T., Mentzel, H.J., Miltner, W.H., 2005. Common and distinct brain activation to threat and safety signals in social phobia. Neuropsychobiology 52, 163–168.
Strick, P.L., Dum, R.P., Fiez, J.A., 2009. Cerebellum and nonmotor function. Annual Review of Neuroscience 32, 413–434.
Tillfors, M., Furmark, T., Marteinsdottir, I., Fischer, H., Pissiota, A., Långström, B., Fredrikson, M., 2001. Cerebral blood flow in subjects with social phobia during stressful speaking tasks: a PET study. American Journal of Psychiatry 158, 1220–1226.
Warwick, J.M., Carey, P., Jordaan, G.P., Dupont, P., Stein, D.J., 2008. Resting brain perfusion in social anxiety disorder: a voxel-wise whole brain comparison with healthy control subjects. Progress in Neuro-psychopharmacology & Biological Psychiatry 32, 1251–1256.
Wechsler, D., 1981. WAIS-R Manual. Psychological Corporation, New York.
Wik, G., Fredrikson, M., Ericson, K., Eriksson, L., Stone-Elander, S., Greitz, T., 1993. A functional cerebral response to frightening visual stimulation. Psychiatry Research 50, 15–24.

FosB Is Essential for the Enhancement of Stress Tolerance and Antagonizes Locomotor Sensitization by ΔFosB

Yoshinori N. Ohnishi, Yoko H. Ohnishi, Masaaki Hokama, Hiroko Nomaru, Katsuhisa Yamazaki, Yohei Tominaga, Kunihiko Sakumi, Eric J. Nestler, and Yusaku Nakabeppu

Background: Molecular mechanisms underlying stress tolerance and vulnerability are incompletely understood. The *fosB* gene is an attractive candidate for regulating stress responses, because ΔFosB, an alternative splice product of the *fosB* gene, accumulates after repeated stress or antidepressant treatments. On the other hand, FosB, the other alternative splice product of the *fosB* gene, expresses more transiently than ΔFosB but exerts higher transcriptional activity. However, the functional differences of these two *fosB* products remain unclear.

Methods: We established various mouse lines carrying three different types of *fosB* allele, wild-type ($fosB^{+}$), *fosB*-null ($fosB^{G}$), and $fosB^{d}$ allele, which encodes ΔFosB but not FosB, and analyzed them in stress-related behavioral tests.

Results: Because $fosB^{+/d}$ mice show enhanced ΔFosB levels in the presence of FosB and $fosB^{d/d}$ mice show more enhanced ΔFosB levels in the absence of FosB, the function of FosB can be inferred from differences observed between these lines. The $fosB^{+/d}$ and $fosB^{d/d}$ mice showed increased locomotor activity and elevated Akt phosphorylation, whereas only $fosB^{+/d}$ mice showed antidepressive-like behaviors and increased E-cadherin expression in striatum compared with wild-type mice. In contrast, *fosB*-null mice showed increased depression-like behavior and lower E-cadherin expression.

Conclusions: These findings indicate that FosB is essential for stress tolerance mediated by ΔFosB. These data suggest that *fosB* gene products have a potential to regulate mood disorder-related behaviors.

Key Words: Bipolar disorders, depression, *fosB* gene, knockout mice, mania, mood disorder

The *fosB* gene has an intron-like sequence in exon 4, which allows alternative splicing and the production of two distinct transcripts, *fosB* and Δ*fosB* messenger RNAs (mRNAs). The latter encodes ΔFosB protein, which lacks the C-terminal 101 aa containing the transactivation domain in the full-length FosB protein (1). We have previously reported that FosB and ΔFosB oppositely regulate Jun transactivity (1,2) and cell matrix adhesion (3) in cultured cells; the proteins also regulate cell proliferation, differentiation, and death (4–8). Interestingly, ΔFosB can act, in vivo and in vitro, as a transcriptional activator or repressor (9,10). An example of the latter is feedback repression of the *c-fos* and *fosB* gene promoters (1,11).

ΔFosB has been shown to be a key modulator of reward-related behaviors in response to drugs of abuse, natural reward, and coping with stress (9,12–17). ΔFosB accumulates progressively after repeated or prolonged dopaminergic-related stimuli or convulsive seizures reflecting its high level of stability, in contrast to FosB, which, like c-Fos, is highly unstable and is expressed transiently (12,18–23). However, functional roles of ΔFosB and FosB in mood-related behaviors are incompletely understood. Induction of ΔFosB in several brain areas appears to mediate decreased sensitivity to the deleterious effects of chronic stress (13,24), while the influence of FosB is completely unknown despite its much higher transactivity (1).

Here, we characterized new *fosB* mutant mice: 1) $fosB^{d/d}$ mice with significantly enhanced expression of ΔFosB but no FosB, 2) *fosB*-null ($fosB^{G/G}$) mice lacking both FosB and ΔFosB, and 3) $fosB^{+/d}$ mice with reduced expression of FosB and enhanced expression of ΔFosB. We found that $fosB^{+/d}$ mice serve as a model for endogenous ΔFosB accumulating conditions and that differences between $fosB^{d/d}$ and *fosB*-null mice reflect the effects of enhanced ΔFosB expression in the absence of FosB. In addition, differences observed between $fosB^{+/d}$ and $fosB^{d/d}$ mice revealed the influence of FosB under ΔFosB accumulating conditions.

Methods and Materials

Generation of Mutant Mice

See Supplement 1.

Mice

Two- to 5-month-old male mice were used in most experiments. $fosB^{d/d}$ mice (F8–14) and $fosB^{G/G}$ mice (F5–9) were obtained from heterozygous intercrosses except for experiments involving haloperidol treatment. Control wild-type mice were littermates of each mutant mouse line. No gross differences were apparent between wild-type and mutant mice. Mice were housed in plastic mouse cages with littermates with standard rodent chow and water ad libitum. Animals were maintained in an air-conditioned, light time-controlled, specific pathogen-free room with a 12-hour light/12-hour dark cycle (light on at 8:00 AM and down at 8:00 PM). The handling and killing of all animals were carried out in accordance with the national prescribed guidelines, and ethical approval for the

From the Division of Neurofunctional Genomics (YNO, YHO, MH, HN, KY, YT, KS, YN), Department of Immunobiology and Neuroscience, Medical Institute of Bioregulation, Kyushu University, Fukuoka, Japan; and Fishberg Department of Neuroscience (YNO, YHO, EJN), Mount Sinai School of Medicine, New York, New York.

Address correspondence to Yusaku Nakabeppu, D.Sc., Kyushu University, Medical Institute of Bioregulation, Department of Immunobiology and Neuroscience, Division of Neurofunctional Genomics, 3-1-1 Maidashi Higashi-ku, Fukuoka, Fukuoka 812-8582, Japan; E-mail: yusaku@bioreg.kyushu-u.ac.jp.

Received Oct 26, 2010; revised Apr 23, 2011; accepted Apr 26, 2011.

0006-3223/$36.00
doi:10.1016/j.biopsych.2011.04.021

studies was granted by the Animal Experiment Committee of Kyushu University.

Immunohistochemistry
See Supplement 1.

Western Blot Analysis
See Supplement 1.

Behavior Analyses
See Supplement 1.

Statistical Analysis
See Supplement 1.

Results

Expression of FosB and ΔFosB in Mutant Mice

fosB gene expression in mutant mice was analyzed with immunohistochemistry and Western blotting. Brain immunohistochemistry of wild-type mice revealed that *fosB* gene expression is greatest in the olfactory bulb, nucleus accumbens (NAc), dorsal striatum, anterior cingulate cortex, dentate gyrus of hippocampus, and cerebral cortex. The regional pattern of *fosB* gene expression in the $fosB^{d/d}$ mice is the same as wild-type mice, but the immunoreactivity (IR) is much higher (Figure 1A–C; Figure S1G,H in Supplement 1). In wild-type mice, the anti-FosB(C), which was raised against amino acids 245 to 315 of the C-terminus of FosB (1), detected FosB only sparsely in NAc and dorsal striatum but substantially in cingulate cortex (Figure S1C,D in Supplement 1). This suggests that the majority of the *fosB* gene expression signal is derived from ΔFosB. FosB IR was undetectable in $fosB^{d/d}$ and $fosB^{G/G}$ mice, and ΔFosB IR was undetectable in $fosB^{G/G}$ mice (Figure S1E,F in Supplement 1).

We next performed quantitative Western blotting of striatal nuclear extracts using anti-FosB (Figure 1D–F). Significantly enhanced expression of ΔFosB and Δ2ΔFosB in $fosB^{d/d}$ and to a lesser extent in $fosB^{+/d}$ mice was confirmed in comparison with wild-type mice. Expression levels of FosB and variant FosB (vFosB) in $fosB^{+/d}$ mice were apparently decreased in comparison with those in wild-type mice, and there was no detectable FosB and vFosB in $fosB^{d/d}$ mice (Figure 1D,F). Variant FosB is thought to be Δ1FosB or Δ2FosB (Figure S1A in Supplement 1). In the $fosB^{+/G}$ mice, the levels of vFosB and Δ2ΔFosB, but not FosB and ΔFosB, were significantly decreased in comparison with those in wild-type mice, and none of those were detected in $fosB^{G/G}$ mice (Figure 1E,F).

These data suggest that $fosB^{+/d}$ mice provide a model of ΔFosB accumulation over long periods of time and that the difference between $fosB^{d/d}$ and $fosB^{+/d}$ mice can disclose the function of FosB under conditions of ΔFosB accumulation. Additionally, the differences observed between $fosB^{d/d}$ and $fosB^{G/G}$ mice and shared traits

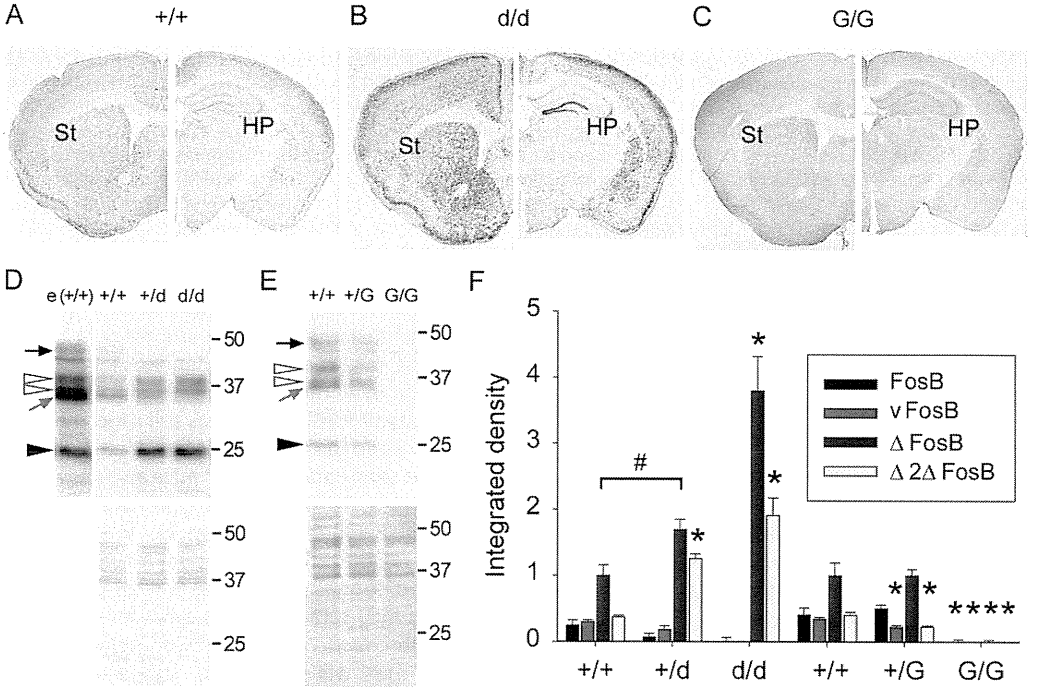

Figure 1. Expression of FosB and ΔFosB in the brain of *fosB* mutant mice. **(A–C)** Immunohistochemical detection of *fosB* gene products in mouse brain. Coronal sections of brain prepared from wild-type, $fosB^{d/d}$, and $fosB^{G/G}$ mice were subjected to immunohistochemistry with anti-FosB(N). The FosB(N) antibody was raised against amino acids 79 to 131 of the N-terminus common to FosB and ΔFosB. Representative sections are shown. The regional distribution of *fosB* gene expression is not different between wild-type and $fosB^{d/d}$ mice, and there is no expression of *fosB* gene products in $fosB^{G/G}$ mice. **(D, E)** Western blotting analysis of *fosB* gene products in striatal nuclear extracts. Blotting membranes were reacted with a rabbit monoclonal anti-FosB (5G4, Cell Signaling Technology, Inc. Danvers, Massachusetts). The black arrow indicates p43 (FosB), the open arrowheads indicate p32/36 (ΔFosB), the red arrow indicates p31 (variant FosB [vFosB]), and the closed arrowhead indicates p24 (Δ2ΔFosB). e(+/+) is enhanced image of wild-type result. The blots were stained with Ponceau S (lower panels in D and E). **(F)** Quantification of FosB, ΔFosB, vFosB, and Δ2ΔFosB bands in striatal samples. Relative values of integrated densities to that of ΔFosB in wild-type mice are shown (n = 3–5, mean ± SEM). Expression levels of ΔFosB and Δ2ΔFosB were increased in $fosB^{+/d}$ and $fosB^{d/d}$ mice compared with wild-type mice [ΔFosB: $F(2,12) = 21.5, p = .0002$; Δ2ΔFosB: $F(2,12) = 24.9, p = .0001$], while those of FosB and vFosB in $fosB^{+/d}$ mice were apparently decreased [FosB: $F(2,12) = 3.54, p = .0689$; vFosB: $F(2,12) = 2.65, p = .119$]. In the $fosB^{+/G}$ mice, the levels of vFosB and Δ2ΔFosB were significantly decreased, and no *fosB* gene product was detected in $fosB^{G/G}$ mice [FosB: $F(2,11) = 10.4$, $p = .0046$; ΔFosB: $F(2,11) = 16.1$, $p = .0011$; vFosB: $F(2,11) = 37.6$, $p < .0001$; Δ2ΔFosB: $F(2,11) = 39.1, p < .0001$]. *$p < .05$ in Dunnett's multiple comparison test. #$p < .05$ in t test. St, striatum; HP, hippocampus.

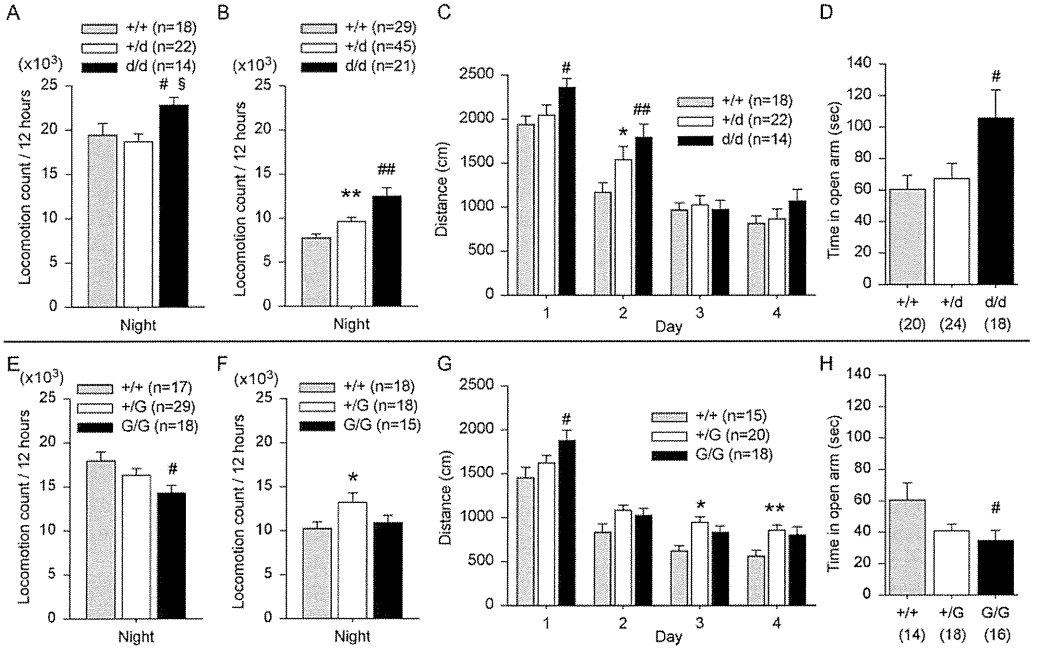

Figure 2. Spontaneous locomotor activity, open field, and elevated plus maze tests in *fosB* mutant mice. Littermates obtained from mating of $fosB^{+/d}$ × $fosB^{+/d}$ (upper panels: **A** to **D**) and $fosB^{+/G}$ × $fosB^{+/G}$ (lower panels: **E** to **H**) mice were used for the experiments. Upper panels represent data of line d (ΔFosB accumulation type). Lower panels represent data of line G (*fosB*-null type). **(A, B, E, F)** Spontaneous locomotor activity during a 12-hour period in the night. Data in panels **(A)** and **(E)** were obtained in the night of the third day after isolation, those in **(B)** and **(F)** after 1 month of isolation. Bars represent locomotor counts per 12 hour (mean ± SEM). On the third night, $fosB^{d/d}$ mice showed significantly higher locomotor activity compared with wild-type and $fosB^{+/d}$ mice [$F(2,51) = 8.82$, $p < .001$], while $fosB^{G/G}$ mice showed significantly lower locomotor activity compared with wild-type mice [$F(2,60) = 3.87$, $p = .026$]. $fosB^{+/d}$ mice also showed significantly higher locomotor activity than wild-type mice ($H = 45.0$, $p < .001$, Kruskal-Wallis test). **(C, G)** Results of the open field test. Bars represent travel distance (cm) for 10 minutes (mean ± SEM). On the first day, both $fosB^{d/d}$ and $fosB^{G/G}$ mice showed significantly higher locomotor activity than wild-type mice [$F(2,51) = 3.56$, $p < .05$ and $F(2,50) = 3.79$, $p < .05$, respectively]. $fosB^{+/d}$ and $fosB^{d/d}$ mice [$F(2,51) = 4.48$, $p < .05$] on the second day and $fosB^{+/G}$ mice [$F(2,50) = 5.96$, $p < .01$, and $F(2,50) = 4.02$, $p < .05$] on the third and fourth days, respectively, exhibited significantly higher locomotor activity than did wild-type mice. **(D, H)** Results of the elevated plus maze test. Bars represent time in open arm (seconds) (mean ± SEM). $fosB^{d/d}$ mice stayed significantly longer in the open arms than wild-type mice ($H = 9.79$, $p = .007$, Kruskal-Wallis test), and $fosB^{G/G}$ mice spent significantly less time in the open arms [$F(2,45) = 4.91$, $p < .01$]. In **(A)** to **(H)**, $^{\#}p < .05$; $^{\#\#}p < .01$; statistical difference between homozygous mutant and wild-type mice. $^{*}p < .05$; $^{**}p < .01$; statistical difference between heterozygous mutant and wild-type mice. $^{\S}p < .05$; statistical difference between heterozygous and homozygous mutant mice, using analysis of variance (Dunnett's post hoc test).

between $fosB^{d/d}$ and $fosB^{+/d}$ mice reflect the results of ΔFosB accumulation.

Higher Spontaneous Locomotor Activity in $fosB^{d/d}$ Mice and Lower Activity in $fosB^{G/G}$ Mice

To infer the function of endogenous ΔFosB and FosB in the central nervous system, we analyzed the two lines of mutant mice and their wild-type littermates in several behavioral assays (Figure 2A–H). Spontaneous locomotor activity was followed through 1 week without any disturbance of individually housed mice in their home cages. The activity of all mice tended to decrease gradually because of the loss of interaction with littermates (Figure S2 in Supplement 1). By the third night, $fosB^{d/d}$ mice showed significantly higher locomotor activity compared with wild-type mice and $fosB^{+/d}$ mice (Figure 2A). On the other hand, $fosB^{G/G}$ mice showed significantly lower locomotor activity compared with wild-type mice (Figure 2E). All mutant mice showed normal levels of locomotor activity at the start of the sleep cycle. These data suggest that ΔFosB facilitates spontaneous motor behavior during periods of wakefulness but does not introduce abnormal motor behavior independent of the circadian cycle. Despite accumulation of comparable levels of ΔFosB in $fosB^{+/d}$ mice, the mice showed lower levels of locomotion compared with that seen in $fosB^{d/d}$ mice, suggesting that FosB suppresses the effect of accumulated ΔFosB and helps to normalize basic locomotion.

We next examined the locomotor activity of mice housed independently for 1 month. Spontaneous locomotion was dramatically decreased in all the genotypes studied. Nevertheless, the locomotor activity of $fosB^{d/d}$ mice was still much higher; in fact, the difference between the activities of $fosB^{d/d}$ and wild-type mice was larger than that seen earlier. $fosB^{+/d}$ mice also showed significantly higher locomotor activity than wild-type mice, suggesting that accumulated ΔFosB enhances spontaneous locomotion (Figure 2B). On the other hand, the difference between $fosB^{G/G}$ and wild-type mice was abolished, suggesting that the level of locomotion after 1 month of isolation may settle down to basal levels without effects of social interaction. $fosB^{+/G}$ mice showed significantly higher locomotor activity than wild-type mice, suggesting that the relatively increased expression level of ΔFosB among all *fosB* gene products in $fosB^{+/G}$ mice may make an effect on the basal locomotor activity (Figure 2F).

Higher Exploratory Activity in Both $fosB^{d/d}$ and $fosB^{G/G}$ Mice but Opposite Behavioral Responses to Fear-Eliciting Stimuli

On the first day in the open field test, which provides a measure of anxiety-like behavior, both $fosB^{d/d}$ and $fosB^{G/G}$ mice showed significantly higher exploratory activity than wild-type mice (Figure 2C,G), suggesting that FosB may increase anxiety-like responses or suppress intrinsic curiosity. Though all the mice showed habituation after the second day of the test, $fosB^{+/d}$ and $fosB^{d/d}$ mice on the

second day and *fosB*$^{+/G}$ mice on the third and fourth days, respectively, exhibited significantly higher locomotor activity than did wild-type mice (Figure 2C,G), suggesting that the difference reflects spontaneous locomotor activity (Figure 2B,F).

In the elevated plus maze, another test of anxiety-like behavior, *fosB*$^{d/d}$ mice stayed significantly longer in the open arms than wild-type mice, and *fosB*$^{G/G}$ mice spent significantly less time in the open arms (Figure 2D,H), suggesting that ΔFosB might suppress anxiety-like behavior and that the presence of FosB may help to normalize it. There was no significant difference in the number of entries into the open and closed arms, but *fosB*$^{d/d}$ mice showed a trend for increased transitions (Figure S3A,C in Supplement 1). In contrast to the open-field and elevated plus maze tests, mutant mice showed no differences in the light-dark test (Figure S3B,D in Supplement 1).

Repeated Forced Swimming in the Morris Water Maze

Next, we used the Morris water maze to evaluate spatial learning ability and found some differences among the mouse lines tested (Figure 3A,B). The swimming speed of the mutant mice showed no difference through the training days (Figure S4C,D in Supplement 1). Interestingly, though the actual swimming time (Figure 3C,D) and distance traveled (Figure S4A,B in Supplement 1) for arrival to the platform were grossly normal, the time to reach the platform was shorter in *fosB*$^{+/d}$ mice and longer in *fosB*$^{G/G}$ mice, especially around the middle of the training days (Figure 3A,B; Table S1 in Supplement 1), because of immobility in the water during training (Figure 3E,F; Table S1 in Supplement 1). In the probe test, all the genotypes spent the longest time in the quadrant where the platform had previously existed (Figure 3G,H; Table S1 in Supplement 1). However, in *fosB*$^{+/G}$ and *fosB*$^{G/G}$ mice, the time was shorter than that in wild-type mice because of immobility in the first quadrant (white boxes in Figure 3G,H).

The forced swim test is used widely as a measure of stress responsiveness, with immobility reflecting greater stress vulnerability. Not surprisingly, the Morris water maze was reported recently to provide useful measures of swim stress responses (25,26). Together, these data suggest that *fosB* gene products do not affect learning ability; however, accumulated ΔFosB decreases stress vulnerability, and such activity requires the presence of FosB.

Repeated Forced Swim Test in Inescapable Condition

Next, to further assess the behavioral responses of *fosB* mutant mice to inescapable stress, we used a conventional forced swim test. We found a trend for decreased swimming time over repeated days of the test in wild-type, *fosB*$^{d/d}$, and *fosB*$^{G/G}$ mice, but not in *fosB*$^{+/d}$ mice (Figure 4). *fosB*$^{d/d}$ and *fosB*$^{G/G}$ mice showed significantly decreased swimming time on the second and third days, respectively. Additionally, we injected the mice with paroxetine (10 mg/kg), a standard antidepressant, 30 minutes before the swim test on the fourth day. Paroxetine increased the swimming time well beyond levels seen on the first day in all types of mice except *fosB*$^{G/G}$ mice. In *fosB*$^{G/G}$ mice, the swimming time recovered but did not reach the level of the first day, and this recovery ratio was significantly lower than that seen in wild-type mice.

Responsivity to Dopamine Signals in Mutant Mice

fosB$^{d/d}$ mice showed hyperlocomotion in the active phase with a normal circadian pattern (Figure S2 and Figure S4A in Supplement 1) but appeared less anxious or fearful in the elevated plus maze (Figure 2D). These behavioral phenotypes are somewhat reminiscent of the symptoms of attention-deficit/hyperactivity disorder (27). Attention-deficit/hyperactivity disorder patients can be treated successfully with methylphenidate (MPH). Methylphenidate inhibits dopamine reuptake and increases the dopamine concentration in synaptic clefts, which leads to hyperlocomotion in healthy individuals. However, attention-deficit/hyperactivity disorder patients calm down in paradoxical reactions to MPH. Therefore, we examined whether MPH exerted therapeutic-like effects in *fosB*$^{d/d}$ mice compared with effects of other dopaminergic drugs (Figure 5A–D; Figure S5 in Supplement 1). We found that MPH induced transient hyperlocomotion (Figure 5A,B), which settled down to baseline within 4 hours after intraperitoneal injection in all types of *fosB* mutant mice and their wild-type littermates (Figure S5C,D in Supplement 1). In particular, *fosB*$^{+/d}$ and *fosB*$^{d/d}$ mice exhibited more hyperactivity in response to MPH than wild-type mice. The transient hyperlocomotion exhibited by *fosB*$^{+/d}$ and *fosB*$^{d/d}$ mice was similar, but the locomotor activity exhibited in the dark phase after MPH treatment was decreased in *fosB*$^{+/d}$ mice (Figure 5A,C). These data suggest that accumulated ΔFosB drives locomotion during the dark phase, while the existence of FosB prevents it (Figure S5C in Supplement 1). *fosB*$^{+/G}$ and *fosB*$^{G/G}$ mice exhibited equivalent reactions to MPH as wild-type mice, suggesting that normal low levels of ΔFosB do not contribute to basal dopamine sensitivity and that only accumulated ΔFosB can facilitate it (Figure 5B; Figure S5B,D in Supplement 1).

Basal ganglia circuitry regulates motor function via two pathways, termed the direct and indirect pathways. More than 90% of striatal neurons are medium spiny γ-aminobutyric acidergic projection neurons. About half of them project directly to the midbrain and express dynorphin and the D1 dopamine receptor; activation of these neurons increases locomotion and induces *fosB* gene expression. The other half indirectly project to the midbrain via the globus pallidus and subthalamic nucleus and express enkephalin and the D2 dopamine receptor; activation of these neurons decreases locomotion (28). D2 receptor signaling in these neurons inhibits such downregulation of locomotion and suppresses *fosB* gene expression (29).

Werme *et al.* (30) reported that ΔFosB overexpression selectively in direct pathway neurons increased daily running compared with control littermates, whereas ΔFosB overexpression predominantly in indirect pathway neurons decreased it. At first, we hypothesized that spontaneous hyperlocomotion and higher responsivity to MPH in *fosB*$^{+/d}$ and *fosB*$^{d/d}$ mice are dependent on increased D1 receptor signaling sensitivity. However, locomotor responses to a D1 receptor agonist (2 mg/kg SKF81297) showed no differences among all the *fosB* mutant and wild-type mice (Figure 5A,B; Figure S5E,F in Supplement 1). Next, we administered a D2 receptor antagonist (1 mg/kg haloperidol), which is reported to induce *fosB* gene expression in D2-containing neurons, as well as hypolocomotion (29,31). The total locomotor activity over 4 hours after haloperidol treatment was significantly higher in *fosB*$^{d/d}$ mice and lower in *fosB*$^{G/G}$ mice compared with wild-type mice (Figure 5A,B; Figure S5G,H in Supplement 1). This finding, along with the pattern of results in the elevated plus maze (Figure 2D,H) and spontaneous locomotion test on the second and third day after isolation from littermates (Figure S2 in Supplement 1), suggests that accumulated ΔFosB suppresses the D2 receptor signal. This, in turn, may contribute to the increased locomotion and reduction in anxiety-like behavior induced by ΔFosB, with FosB negatively regulating the effects of accumulated ΔFosB.

We detected no behavioral differences in the effects of a D2 agonist (1 mg/kg LY171555) among the *fosB* mutant and wild-type mice (Figure 5A,B,; Figure S5I,J in Supplement 1). These data suggest that, in the mutant mice, negative feedback via D2 receptors on dopamine neurons in the midbrain may function normally (32).

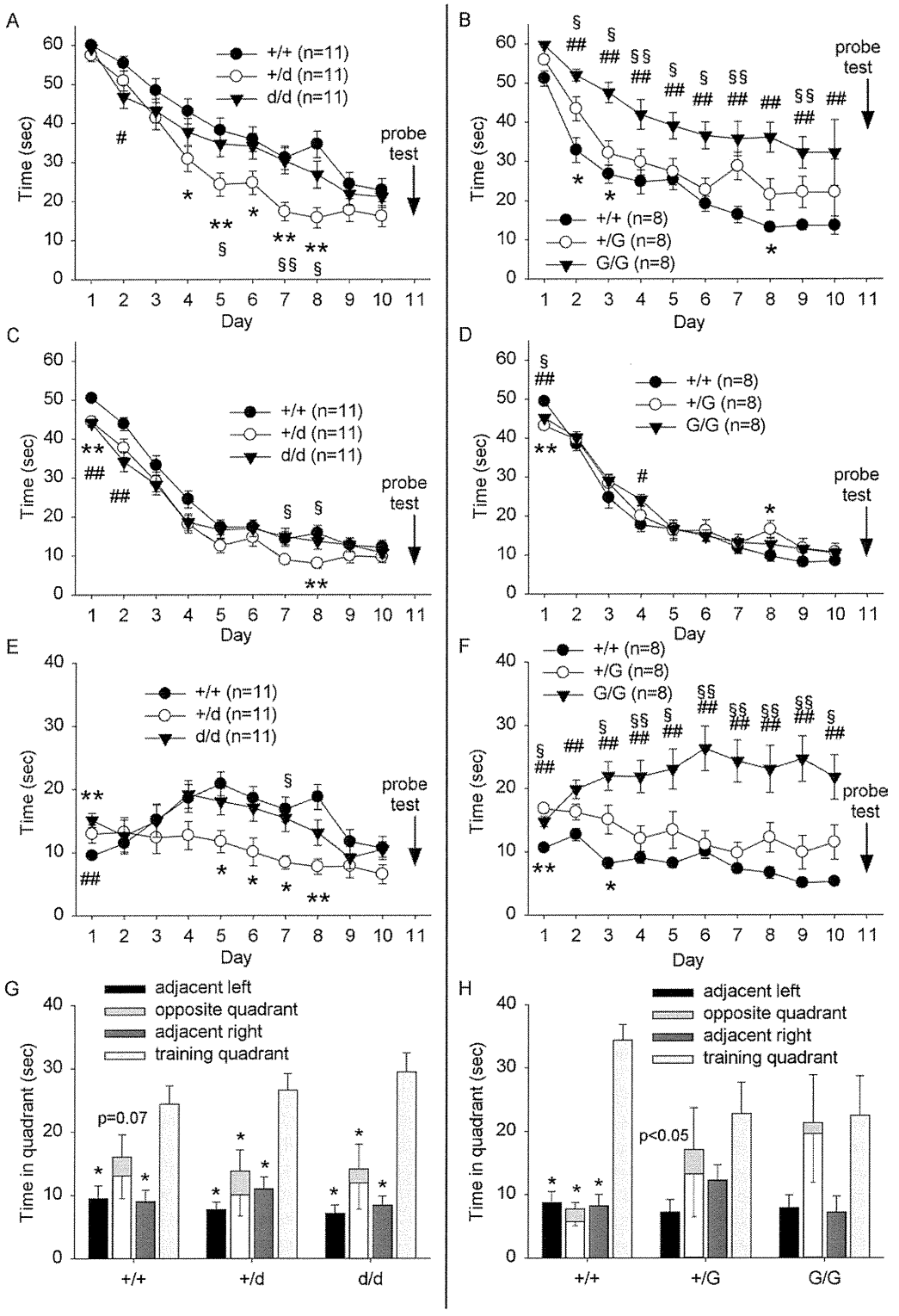

Figure 3. Repeated forced swimming in the Morris water maze in *fosB* mutant mice. Left panels represent data of line d (ΔFosB accumulation type). Right panels represent data of line G (*fosB*-null type). **(A, B)** Escape latency in the hidden platform test. **(C, D)** Actual swimming time exhibited no gross differences in the mutant mice. **(E, F)** Immobility time in the water maze contributed the difference in time to reach the hidden platform. In **(A–F)**, all points are shown as mean ± SEM. $^{\#}p < .05$; $^{\#\#}p < .01$; statistical difference between homozygous mutant and wild-type mice. $^{*}p < .05$; $^{**}p < .01$; statistical difference between heterozygous mutant and wild-type mice. $^{\S}p < .05$; $^{\S\S}p < .01$; statistical difference between heterozygous and homozygous mutant mice, using analysis of variance (Dunnett's post hoc test) **(G, H)** Time in each quadrant in probe test at 11th day after 10 days training. The white box in the opposite quadrant reflects the time until moving to the other quadrant from the first quadrant. $^{*}p < .01$; comparison with the training quadrant, using analysis of variance (Dunnett's post hoc test).

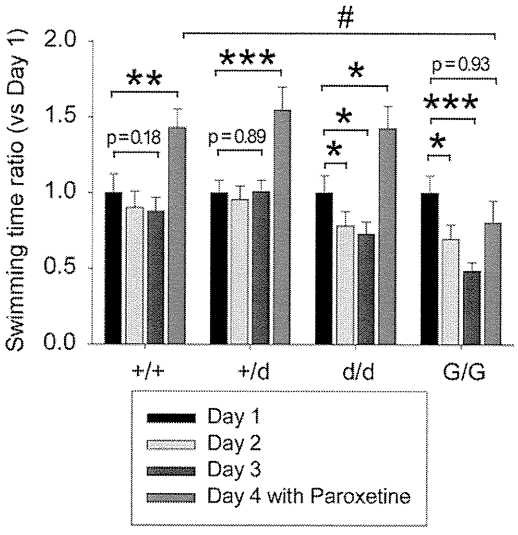

Figure 4. Repeated forced swim test of *fosB* mutant mice in inescapable condition. Conventional repeated forced swim test was performed once a day for 4 consecutive days. Each trial was performed for 6 minutes, and relative ratio of swimming time during last 4 minutes on a given day to that in the day 1 is shown in a bar graph (mean ± SEM, $n = 12–16$). Paroxetine (10 mg/kg) was injected 30 minutes before the fourth day trial. In $fosB^{G/G}$ mice, the recovery ratio of the swimming time after administration of paroxetine was significantly lower than that seen in wild-type mice [$F(3,56) = 3.11$, $p < .05$]. *$p < .05$; **$p < .01$; ***$p < .001$; statistical difference between the day 1 and a given day in each mouse line. #$p < .05$; statistical difference between $fosB^{G/G}$ and wild-type mice using analysis of variance (Dunnett's post hoc test).

E-Cadherin Expression Levels Parallel Stress Responses and *fosB* Gene Expression

To further elucidate how *fosB* gene products regulate complex behavior, we selectively picked several postulated target proteins from previous reports (3,14,33) and then performed Western blotting with striatum samples (Figure S6A in Supplement 1). E-cadherin was significantly upregulated in $fosB^{+/d}$ mice and downregulated in $fosB^{+/G}$ and $fosB^{G/G}$ mice; in other words, the expression level of E-cadherin paralleled the behavioral phenotype of stress tolerance seen with forced swimming. Similar tendencies were detected in hippocampus (data not shown). In contrast, there was no difference in the expression levels of cyclin-dependent kinase 5, glutamate receptor type 2 (GluR2), α-catenin, or β-catenin (the first two are putative ΔFosB targets identified in bitransgenic mice, and the latter two are binding partners of E-cadherin) among *fosB* mutant and wild-type mice (Figure S6A in Supplement 1). The level of E-cadherin mRNA in NAc also showed no difference among mutant and wild-type mice (data not shown), suggesting that the upregulation of E-cadherin is regulated by posttranslational mechanisms.

Akt Phosphorylation Is Increased by ΔFosB Accumulation

Finally, we checked the level of Akt and its phosphorylation in the striatum of *fosB* mutant mice (Figure S6B in Supplement 1). Total Akt protein levels showed no difference among mutant and wild-type mice, but the phosphorylation state of Akt (T308) was significantly elevated in $fosB^{+/d}$ and $fosB^{d/d}$ mice.

Discussion

In this study, we provide evidence that accumulated ΔFosB increases locomotor activity and that FosB antagonizes this effect similar to findings from in vitro cellular assays (1). On the other hand, stress tolerance appears to be the sum of ΔFosB and FosB. These effects may be partly mediated via E-cadherin, an indirect target of *fosB* gene products. Together, these data suggest distinct patterns of behavioral abnormalities among the mutant mouse lines examined (Figure 6). We propose that $fosB^{G/G}$ mice exhibit behaviors that resemble depression, including decreased locomotion, increased immobility during forced swimming, and increased anxiety-like responses. In contrast, $fosB^{+/d}$ mice exhibit behaviors that in some ways resemble manic-like symptoms, including hyperlocomotion, increased stress tolerance, and reduced anxiety-like responses. Interestingly, $fosB^{d/d}$ mice exhibit significantly higher dopamine sensitivity and most of the altered behaviors seen in $fosB^{+/d}$ mice except for increased stress tolerance. These mice thus present a picture of blended responses perhaps reminiscent of certain aspects of bipolar disorder. Clearly, these interpretations are based on initial analyses in rodent models and require much further work for validation, including studying these molecular findings in the human disorders.

The similar results obtained from $fosB^{G/G}$ mice in the water maze (Figure 3) and repeated forced swim test (Figure 4) indicate that the water maze has the potential to reveal responses to stress. Whereas the repeated forced swim test revealed the stress vulnerability of $fosB^{d/d}$ mice more clearly than the water maze, the difference between wild-type and $fosB^{+/d}$ mice was more apparent in the water maze, suggesting that the repeated forced swim test may be better to detect initial stress vulnerability, while the water maze may be better to detect stress tolerance that develops over time. Data with paroxetine suggest that *fosB* gene products are partly required for antidepressant responses to the drug, as reported recently (24).

In $fosB^{+/d}$ mice, the antagonistic relationship between FosB and accumulated ΔFosB, first seen in vitro (1), was captured in measures of spontaneous locomotor activity (Figure 2A; Figure S2A in Supplement 1), elevated plus maze (Figure 2D), and sensitivity to a D2 antagonist (Figure 5A; Figure S5G in Supplement 1). The expression level of ΔFosB in $fosB^{+/d}$ mice is much higher than that of FosB, but FosB has much higher transactivity than ΔFosB (1,34). These data suggest that lower expression levels of FosB may be sufficient to suppress the activity of accumulated ΔFosB and thereby normalize some of the consequences of its accumulation (Figure S7 in Supplement 1). Such antagonism is not seen in all cases, perhaps reflecting the different cell types or target genes involved. In ΔFosB bitransgenic mice, where ΔFosB expression is inducible and relatively restricted to D1 neurons in NAc and dorsal striatum, Kelz *et al.* (14) reported higher locomotor activity in a novel test chamber on the second day but not on the first day. This finding corresponds to observations in $fosB^{+/d}$ mice, which exhibited higher locomotor activity with a similar pattern (Figure 2C), thus suggesting that ΔFosB accumulation in striatum plays an important role in mediating locomotor activation via dopamine signaling.

We know that the *fosB* gene is induced by dopaminergic signals (23). Because Akt phosphorylation is also induced by dopamine (35), it is possible that accumulated ΔFosB enhances Akt phosphorylation and that the extent of spontaneous dopaminergic activation reflects levels of Akt phosphorylation. Perrotti *et al.* (23) reported that morphine induces ΔFosB accumulation in NAc, and Russo *et al.* (36) reported that overexpression of a constitutively active form of Akt in NAc enhances locomotor sensitization induced by morphine. Locomotor sensitization by morphine is regulated by indirect dopaminergic mechanisms such as increased dopamine release in NAc (37,38). Cocaine directly increases dopamine release in NAc by inhibiting dopamine reuptake. Overexpression of ΔFosB enhanced cocaine locomotor sensitization (39), suggesting that enhanced Akt phosphorylation by accumulated ΔFosB might facilitate locomotor sensitization by cocaine and by morphine. This is

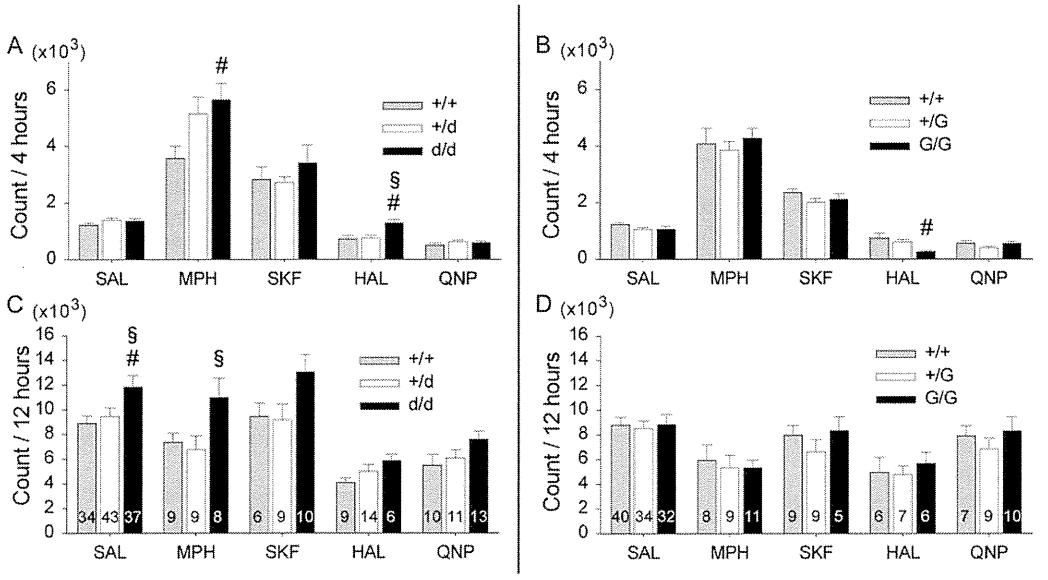

Figure 5. Locomotor activity induced by dopamine receptor agonists and antagonists in *fosB* mutant mice. Left panels represent data of line d (ΔFosB accumulation type). Right panels represent data of line G (*fosB*-null type). Naive mice, without prior behavioral assays, were housed individually for 2 weeks and then placed in a cage with an infrared automatic monitor system for 3 days. On the second day at 4:00 PM, the mice were injected with saline (SAL), and on the third day at 4:00 PM, the mice were injected with 30 mg/kg methylphenidate (MPH), 2 mg/kg SKF81297 (SKF), 1 mg/kg haloperidol (HAL), or 1 mg/kg LY171555 (QNP) as shown in Figure S5 in Supplement 1. **(A, B)** Immediate effects on locomotor activity during the first 4 hours after treatment. Bars represent locomotor counts observed during the first 4 hours from 4:00 PM to 8:00 PM (mean ± SEM). $fosB^{+/d}$ and $fosB^{d/d}$ mice exhibited more hyperactivity in response to MPH than wild-type mice [$F(2,23) = 4.14$, $p < .05$]. The total locomotor activity immediately after haloperidol treatment was significantly higher in $fosB^{d/d}$ mice [$F(2,29) = 4.95$, $p < .05$] and lower in $fosB^{G/G}$ mice [$F(2,16) = 7.43$, $p < .01$], compared with wild-type mice. **(C, D)** Delayed effects on locomotor activity. Bars represent locomotor counts observed during the last 12 hours from 8:00 PM to 8:00 AM the next day (mean ± SEM). The locomotor activity exhibited in the dark phase after MPH treatment was decreased in $fosB^{+/d}$ mice [$F(2,23) = 3.78$, $p < .05$]. In **(A)** to **(D)**, $^{\#}p < .05$; statistical difference between homozygous mutant and wild-type mice, $^{\S}p < .05$; statistical difference between heterozygous and homozygous mutant mice, using analysis of variance (Dunnett's post hoc test). The number of mice is provided in Figure S5 in Supplement 1.

consistent with the significant upregulation of Akt phosphorylation and enhanced locomotor sensitization by MPH observed in $fosB^{d/d}$ mice (Figure 5A; Figure S6C in Supplement 1). The mechanism by which ΔFosB accumulation leads to increased Akt phosphorylation is not known, because ΔFosB could affect the expression of any of several regulators of Akt phosphorylation (40). One possibility is that accumulated ΔFosB may repress the expression of a protein phosphatase, such as PP2A, because Akt phosphorylation is known to be suppressed by D2 signaling in striatum via the activation of this phosphatase (41). These and other possibilities now require direct investigation.

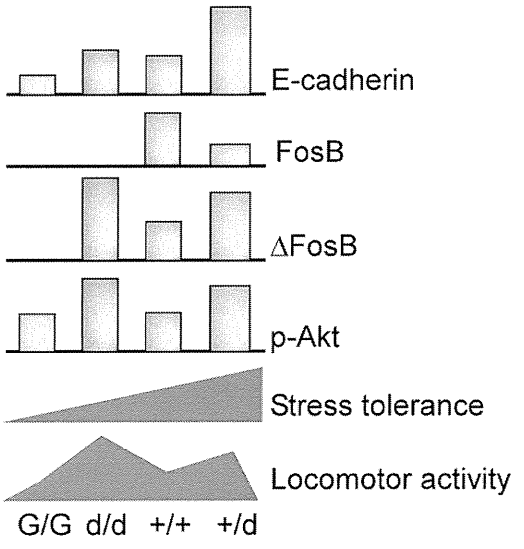

Figure 6. Summary of the effects of different levels of *fosB* gene products on locomotor activity and stress tolerance. FosB and accumulated ΔFosB amplify stress tolerance and E-cadherin expression cooperatively. Accumulated ΔFosB facilitates Akt phosphorylation and locomotor activity thorough its dopaminergic sensitization, while FosB antagonizes the effects.

fosB-knockout (KO) mice had been established by Brown *et al.* (42) and actually have a potential to express Δ3ΔFosB, an alternative-translation initiation product similar to Δ2ΔFosB (Figure S1 in Supplement 1). Hiroi *et al.* (12) and Zhu *et al.* (43) reported that *fosB*-KO mice showed slightly higher locomotor activity when they were introduced into a novel test chamber. This corresponds to our observation that $fosB^{G/G}$ mice exhibit significantly higher locomotor activity in the open field on the first day (Figure 2G), suggesting that FosB may suppress exploratory behavior in the novel environment independent of the presence of ΔFosB. On the other hand, Zhu *et al.* (43) reported that the *fosB*-KO mice exhibit lower sensitivity to other types of stress paradigms (tail suspension test), and Brown *et al.* (42) reported that the *fosB*-KO mice exhibit a defect in nurturing and no difference in the Morris water maze test. These findings are not consistent with our results, because $fosB^{G/G}$ mice exhibited higher stress vulnerability and no defect in nurturing (data not shown). These differences could reflect the potential influence of Δ3ΔFosB or the different genetic backgrounds (BALB/c in the prior studies by Brown *et al.* [42] and C57BL6/J in the present investigations).

Interestingly, the expression level of E-cadherin and the stress tolerance observed on repeated forced swimming paralleled the combined expression of FosB and ΔFosB. Only with regard to the particular expression pattern and behavioral phenotype does FosB

not antagonize but coordinates with ΔFosB. ΔFosB has been reported to accumulate after chronic stress in several brain regions (22,24), and accumulated ΔFosB in the ventrolateral periaqueductal gray promotes active coping responses against stress, such as forced swimming (13). More recently, overexpression of ΔFosB in the NAc suppresses the deleterious effects of social defeat (24). Findings from the present study suggest that such antidepressant-like effects of ΔFosB require the presence of FosB.

E-cadherin is an important cell-cell adhesion molecule and influences synapse formation in neuronal cells (44). In rodent models of depression, the number of mature synapse buttons or dendritic spines is decreased for several neuronal cell types, and antidepressant treatments reverse these abnormalities (45–47). Here, we found that the expression level of E-cadherin in *fosB* mutant and wild-type mice parallels stress tolerance, suggesting that E-cadherin may be one mechanism underlying the stress tolerance induced by *fosB* gene products. FosB might inhibit E-cadherin degradation via transactivation of an inhibitory binding protein against Hakai, which is an E3-ligase of E-cadherin, or directly inhibit the transcription of Hakai mRNA (48). Accumulated ΔFosB might increase E-cadherin translation via transforming growth factor-β signaling, which is increased in $fosB^{+/d}$ and $fosB^{d/d}$ embryonic stem cells (3). Future studies are needed to explore these possibilities directly.

Cyclin-dependent kinase 5 and GluR2, putative ΔFosB targets identified in bitransgenic mouse models (14,33,49), are expressed at similar levels among *fosB* mutants and wild-type mice (Ohnishi et al., unpublished data). McClung and Nestler (9) reported that the expression levels of various ΔFosB targets in these mice switched from upregulated to downregulated, or vice versa, between 2 and 8 weeks after turning on ΔFosB expression. The constitutive changes in *fosB* gene expression in our mutant mice might not result in altered expression of cyclin-dependent kinase 5 and GluR2.

In summary, the $fosB^{G/G}$ mutant is a definitive *fosB*-null mouse, and $fosB^{+/d}$ and $fosB^{d/d}$ mutants differentially express aberrant levels of ΔFosB and FosB from the endogenous *fosB* gene. These three mouse lines exhibit behavioral abnormalities mimicking different types of mood disorders. Further studies of these mice will shed light on the mechanisms controlling mood disorder-related behaviors and thus contributing to the development of improved treatments for these disorders.

This work was supported by grants from Core Research for Evolutional Science and Technology, Japan Science and Technology Agency, the Ministry of Education, Culture, Sports, Science, and Technology of Japan (Grant number: 16012248) and the Japan Society for the Promotion of Science (Grants 16390119 and 18300124, 22221004).

We thank Dr. M. Katsuki (National Institutes of Natural Sciences, Tokyo, Japan) for CCE embryonic stem cells, M. Otsu in the Laboratory for Technical Support, Medical Institute of Bioregulation, for the DNA sequence analyses, A. Matsuyama and K. Nakabeppu for animal care, and S. Kitamura for tissue processing. We also thank all members of our laboratory for their helpful discussions.

The authors report no biomedical financial interests or potential conflicts of interest.

Supplementary material cited in this article is available online.

1. Nakabeppu Y, Nathans D (1991): A naturally occurring truncated form of FosB that inhibits Fos/Jun transcriptional activity. *Cell* 64:751–759.
2. Nakabeppu Y, Nathans D (1989): The basic region of Fos mediates specific DNA binding. *EMBO J* 8:3833–3841.
3. Ohnishi YN, Sakumi K, Yamazaki K, Ohnishi YH, Miura T, Tominaga Y, Nakabeppu Y (2008): Antagonistic regulation of cell-matrix adhesion by FosB and ΔFosB/Δ2ΔFosB encoded by alternatively spliced forms of *fosB* transcripts. *Mol Biol Cell* 19:4717–4729.
4. Kurushima H, Ohno M, Miura T, Nakamura TY, Horie H, Kadoya T, *et al.* (2005): Selective induction of ΔFosB in the brain after transient forebrain ischemia accompanied by an increased expression of galectin-1, and the implication of ΔFosB and galectin-1 in neuroprotection and neurogenesis. *Cell Death Differ* 12:1078–1096.
5. Miura T, Ohnishi Y, Kurushima H, Horie H, Kadoya T, Nakabeppu Y (2005): Regulation of the neuronal fate by ΔFosB and its downstream target, galectin-1. *Curr Drug Targets* 6:437–444.
6. Nakabeppu Y, Oda S, Sekiguchi M (1993): Proliferative activation of quiescent Rat-1A cells by ΔFosB. *Mol Cell Biol* 13:4157–4166.
7. Nishioka T, Sakumi K, Miura T, Tahara K, Horie H, Kadoya T, Nakabeppu Y (2002): FosB gene products trigger cell proliferation and morphological alteration with an increased expression of a novel processed form of galectin-1 in the rat 3Y1 embryo cell line. *J Biochem* 131:653–661.
8. Tahara K, Tsuchimoto D, Tominaga Y, Asoh S, Ohta S, Kitagawa M, *et al.* (2003): ΔFosB, but not FosB, induces delayed apoptosis independent of cell proliferation in the Rat1a embryo cell line. *Cell Death Differ* 10:496–507.
9. McClung CA, Nestler EJ (2003): Regulation of gene expression and cocaine reward by CREB and ΔFosB. *Nat Neurosci* 6:1208–1215.
10. Renthal W, Kumar A, Xiao G, Wilkinson M, Covington HE, 3rd, Maze I, *et al.* (2009): Genome-wide analysis of chromatin regulation by cocaine reveals a role for sirtuins. *Neuron* 62:335–348.
11. Renthal W, Carle TL, Maze I, Covington HE 3rd, Truong HT, Alibhai I, *et al.* (2008): Delta FosB mediates epigenetic desensitization of the *c-fos* gene after chronic amphetamine exposure. *J Neurosci* 28:7344–7349.
12. Hiroi N, Brown JR, Haile CN, Ye H, Greenberg ME, Nestler EJ (1997): FosB mutant mice: Loss of chronic cocaine induction of Fos-related proteins and heightened sensitivity to cocaine's psychomotor and rewarding effects. *Proc Natl Acad Sci U S A* 94:10397–10402.
13. Berton O, Covington HE 3rd, Ebner K, Tsankova NM, Carle TL, Ulery P, *et al.* (2007): Induction of ΔFosB in the periaqueductal gray by stress promotes active coping responses. *Neuron* 55:289–300.
14. Kelz MB, Chen J, Carlezon WA Jr, Whisler K, Gilden L, Beckmann AM, *et al.* (1999): Expression of the transcription factor ΔFosB in the brain controls sensitivity to cocaine. *Nature* 401:272–276.
15. Nestler EJ (2008): Transcriptional mechanisms of addiction: Role of ΔFosB. *Philos Trans R Soc B* 363:3245–3255.
16. Wallace DL, Vialou V, Rios L, Carle-Florence TL, Chakravarty S, Kumar A, *et al.* (2008): The influence of ΔFosB in the nucleus accumbens on natural reward-related behavior. *J Neurosci* 28:10272–10277.
17. Zachariou V, Bolanos CA, Selley DE, Theobald D, Cassidy MP, Kelz MB, *et al.* (2006): An essential role for ΔFosB in the nucleus accumbens in morphine action. *Nat Neurosci* 9:205–211.
18. Hiroi N, Marek GJ, Brown JR, Ye H, Saudou F, Vaidya VA, *et al.* (1998): Essential role of the *fosB* gene in molecular, cellular, and behavioral actions of chronic electroconvulsive seizures. *J Neurosci* 18:6952–6962.
19. Herdegen T, Leah JD (1998): Inducible and constitutive transcription factors in the mammalian nervous system: Control of gene expression by Jun, Fos and Krox, and CREB/ATF proteins. *Brain Res Brain Res Rev* 28:370–490.
20. McClung CA, Ulery PG, Perrotti LI, Zachariou V, Berton O, Nestler EJ (2004): ΔFosB: A molecular switch for long-term adaptation in the brain. *Brain Res Mol Brain Res* 132:146–154.
21. Nestler EJ, Kelz MB, Chen J (1999): ΔFosB: A molecular mediator of long-term neural and behavioral plasticity. *Brain Res* 835:10–17.
22. Perrotti LI, Hadeishi Y, Ulery PG, Barrot M, Monteggia L, Duman RS, Nestler EJ (2004): Induction of ΔFosB in reward-related brain structures after chronic stress. *J Neurosci* 24:10594–10602.
23. Perrotti LI, Weaver RR, Robison B, Renthal W, Maze I, Yazdani S, *et al.* (2008): Distinct patterns of ΔFosB induction in brain by drugs of abuse. *Synapse* 62:358–369.
24. Vialou V, Robison AJ, Laplant QC, Covington HE 3rd, Dietz DM, Ohnishi YN, *et al.* (2010): ΔFosB in brain reward circuits mediates resilience to stress and antidepressant responses. *Nat Neurosci* 13:745–752.
25. Schulz D, Huston JP, Buddenberg T, Topic B (2007): "Despair" induced by extinction trials in the water maze: Relationship with measures of anxiety in aged and adult rats. *Neurobiol Learn Mem* 87:309–323.
26. Schulz D, Topic B, De Souza Silva MA, Huston JP (2004): Extinction-induced immobility in the water maze and its neurochemical concom-

itants in aged and adult rats: A possible model for depression? *Neurobiol Learn Mem* 82:128–141.
27. van der Kooij MA, Glennon JC (2007): Animal models concerning the role of dopamine in attention-deficit hyperactivity disorder. *Neurosci Biobehav Rev* 31:597–618.
28. Gerfen CR, Engber TM, Mahan LC, Susel Z, Chase TN, Monsma FJ Jr, Sibley DR (1990): D1 and D2 dopamine receptor-regulated gene expression of striatonigral and striatopallidal neurons. *Science* 250:1429–1432.
29. Doucet JP, Nakabeppu Y, Bedard PJ, Hope BT, Nestler EJ, Jasmin BJ, *et al.* (1996): Chronic alterations in dopaminergic neurotransmission produce a persistent elevation of ΔFosB-like protein(s) in both the rodent and primate striatum. *Eur J Neurosci* 8:365–381.
30. Werme M, Messer C, Olson L, Gilden L, Thorén P, Nestler EJ, Brené S (2002): ΔFosB regulates wheel running. *J Neurosci* 22:8133–8138.
31. Hiroi N, Graybiel AM (1996): Atypical and typical neuroleptic treatments induce distinct programs of transcription factor expression in the striatum. *J Comp Neurol* 374:70–83.
32. Tang L, Todd RD, O'Malley KL (1994): Dopamine D2 and D3 receptors inhibit dopamine release. *J Pharmacol Exp Ther* 270:475–479.
33. Chen J, Zhang Y, Kelz MB, Steffen C, Ang ES, Zeng L, Nestler EJ (2000): Induction of cyclin-dependent kinase 5 in the hippocampus by chronic electroconvulsive seizures: Role of ΔFosB. *J Neurosci* 20:8965–8971.
34. Ulery PG, Nestler EJ (2007): Regulation of ΔFosB transcriptional activity by Ser27 phosphorylation. *Eur J Neurosci* 25:224–230.
35. Brami-Cherrier K, Valjent E, Garcia M, Pagès C, Hipskind RA, Caboche J (2002): Dopamine induces a PI3-kinase-independent activation of Akt in striatal neurons: A new route to cAMP response element-binding protein phosphorylation. *J Neurosci* 22:8911–8921.
36. Russo SJ, Bolanos CA, Theobald DE, DeCarolis NA, Renthal W, Kumar A, *et al.* (2007): IRS2-Akt pathway in midbrain dopamine neurons regulates behavioral and cellular responses to opiates. *Nat Neurosci* 10:93–99.
37. Leone P, Pocock D, Wise RA (1991): Morphine-dopamine interaction: Ventral tegmental morphine increases nucleus accumbens dopamine release. *Pharmacol Biochem Behav* 39:469–472.
38. Zarrindast MR, Zarghi A (1992): Morphine stimulates locomotor activity by an indirect dopaminergic mechanism: Possible D-1 and D-2 receptor involvement. *Gen Pharmacol* 23:1221–1225.
39. Ulery-Reynolds PG, Castillo MA, Vialou V, Russo SJ, Nestler EJ (2009): Phosphorylation of ΔFosB mediates its stability in vivo. *Neuroscience* 158:369–372.
40. Franke TF (2008): PI3K/Akt: Getting it right matters. *Oncogene* 27:6473–6488.
41. Beaulieu JM, Sotnikova TD, Marion S, Lefkowitz RJ, Gainetdinov RR, Caron MG (2005): An Akt/beta-arrestin 2/PP2A signaling complex mediates dopaminergic neurotransmission and behavior. *Cell* 122: 261–273.
42. Brown JR, Ye H, Bronson RT, Dikkes P, Greenberg ME (1996): A defect in nurturing in mice lacking the immediate early gene *fosB*. *Cell* 86:297–309.
43. Zhu H, Lee M, Agatsuma S, Hiroi N (2007): Pleiotropic impact of constitutive *fosB* inactivation on nicotine-induced behavioral alterations and stress-related traits in mice. *Hum Mol Genet* 16:820–836.
44. Togashi H, Abe K, Mizoguchi A, Takaoka K, Chisaka O, Takeichi M (2002): Cadherin regulates dendritic spine morphogenesis. *Neuron* 35:77–89.
45. McEwen BS (2005): Glucocorticoids, depression, and mood disorders: Structural remodeling in the brain. *Metabolism* 54:20–23.
46. Norrholm SD, Ouimet CC (2001): Altered dendritic spine density in animal models of depression and in response to antidepressant treatment. *Synapse* 42:151–163.
47. Nestler EJ, Barrot M, DiLeone RJ, Eisch AJ, Gold SJ, Monteggia LM (2002): Neurobiology of depression. *Neuron* 34:13–25.
48. Pece S, Gutkind JS (2002): E-cadherin and Hakai: Signalling, remodeling or destruction? *Nat Cell Biol* 4:E72–E74.
49. Peakman MC, Colby C, Perrotti LI, Tekumalla P, Carle T, Ulery P, *et al.* (2003): Inducible, brain region-specific expression of a dominant negative mutant of c-Jun in transgenic mice decreases sensitivity to cocaine. *Brain Res* 970:73–86.

J Mol Neurosci (2011) 44:103–114
DOI 10.1007/s12031-010-9490-2

Cancer-Related PRUNE2 Protein Is Associated with Nucleotides and Is Highly Expressed in Mature Nerve Tissues

Eiji Iwama · Daisuke Tsuchimoto · Teruaki Iyama · Kunihiko Sakumi · Akira Nakagawara · Koichi Takayama · Yoichi Nakanishi · Yusaku Nakabeppu

Received: 18 May 2010 / Accepted: 28 December 2010 / Published online: 14 January 2011

Abstract Human PRUNE is thought to enhance the metastasis of tumor cells. We found that a hypothetical paralog of PRUNE, PRUNE2, binds to 8-oxo-GTP, an oxidized form of GTP. Hypothetical *PRUNE2* gene consists of *C9orf65* and *BMCC1/BNIPXL*, both of which are malignant tumor-associated genes. We isolated *PRUNE2* complementary DNA and revealed that the protein is composed of 3,062 residues. *C9orf65* and *BMCC1/BNIPXL* encode the N-terminal part (259 residues) and C-terminal part (2,729 residues) of PRUNE2, respectively. We demonstrated the endogenous full-length PRUNE2 protein (338 kDa) by Western blot and mass spectrometry. PRUNE2 bound to 8-oxo-GTP as well as GTP. The expression levels of human *PRUNE2* and mouse *Prune2* messenger RNA (mRNA) were highest in the dorsal root ganglia (DRG) and, to a lesser extent, in other nerve tissues. DRG neurons express higher levels of PRUNE2 in their soma compared with adjacent cells. In addition, their expression levels in the adult nerve tissues were higher than those in fetal or neonatal nerve tissues. The present study indicates that *C9orf65* and *BMCC1/BNIPXL* are transcribed as *PRUNE2* mRNA, which is translated to a large PRUNE2 protein. The nerve tissue-specific and post-development expression of *PRUNE2/Prune2* suggests that PRUNE2 may contribute to the maintenance of mature nervous systems.

Keywords PRUNE2 · BMCC1/BNIPXL · C9orf65 · Neuroblastoma · Dorsal root ganglion · 8-Oxo-GTP

Introduction

Nucleotides, which function as regulatory molecules for various cellular metabolism components and precursors for DNA and RNA, are at high risk for oxidation by reactive oxygen species, which are generated by normal metabolism or by the exposure to ionizing radiation or chemicals (Nakabeppu et al. 2006a, b). 8-Oxo-dGTP, an oxidized form of dGTP, is known to cause mutagenesis and cell death. GTP, which is important for intracellular signaling via trimeric or small G proteins, is oxidized to 8-oxo-GTP. However, little is known of its effects on cellular functions.

To explore the effects of 8-oxo-GTP on the functions of cellular proteins, we performed a comprehensive screen of 8-oxo-GTP-binding proteins in an extract of mouse thymocytes and detected a polypeptide corresponding to the N-terminal region of mouse PRUNE2 (NP_851993.3), a hypothetical protein encoded by a gene located on chromosome 19. The human genome is also expected to have a hypothetical ortholog (CAI39749.3), human *PRUNE2*, on chromosome 9. However, N-terminal and C-terminal portions of human PRUNE2 were reported to be encoded by two different genes, *C9orf65* (Price et al. 2007)

Electronic supplementary material The online version of this article (doi:10.1007/s12031-010-9490-2) contains supplementary material, which is available to authorized users.

E. Iwama · D. Tsuchimoto (✉) · T. Iyama · K. Sakumi · Y. Nakabeppu
Division of Neurofunctional Genomics,
Department of Immunobiology and Neuroscience,
Medical Institute of Bioregulation, Kyushu University,
3-1-1 Maidashi, Higashi-ku,
Fukuoka 812-8582, Japan
e-mail: daisuke@bioreg.kyushu-u.ac.jp

E. Iwama · K. Takayama · Y. Nakanishi
Institute of Diseases of the Chest, Kyushu University,
3-1-1 Maidashi, Higashi-ku,
Fukuoka 812-8582, Japan

A. Nakagawara
Division of Biochemistry, Chiba Cancer Center Research Institute,
666-2 Nitona, Chuoh-ku,
Chiba 260-8717, Japan

and *BMCC1* (Machida et al. 2006), respectively. The expression level of *C9orf65* messenger RNA (mRNA) is high in intestinal leiomyosarcoma (LMS) and low in gastrointestinal stromal tumor (GIST), suggesting that *C9orf65* mRNA is a useful marker to distinguish these diseases (Price et al. 2007). On the other hand, *BMCC1* was reported to be preferentially expressed in favorable neuroblastoma (Machida et al. 2006). More recently, it was shown that a BNIP2 and cdc42GAP homology (BCH) domain of BMCC1 suppresses the transformation of cultured cells initiated by Lbc, a RhoA-specific guanine nucleotide exchange factor (RhoGEF), via binding to Rho family proteins (Soh and Low 2008). In the present study, we isolated complementary DNA (cDNA) clones for the full-length PRUNE2 protein and demonstrated the expression of endogenous full-length PRUNE2 protein.

Materials and Methods

Cell Culture

HeLa MR and HEK293T cells were cultured as described previously (Torisu et al. 2005; Tsuchimoto et al. 2001). SH-SY5Y, derived from a neuroblastoma (Biedler et al. 1973), was purchased from American Type Culture Collection (Manassas, VA, USA) and cultured in Dulbecco's modified Eagle's medium (DMEM)/F12 (1:1) (Invitrogen, Carlsbad, CA, USA) supplemented with 10% fetal bovine serum (FBS). KNS81, derived from human glioblastoma (Iida et al. 2004), was cultured in DMEM supplemented with 5% FBS. SK-N-AS, SK-N-BE, IMR32, and RTBM1 cells were cultured as described previously (Machida et al. 2006). NB-1 was obtained from the Japanese Collection of Research Bioresources (Ibaraki, Japan) and cultured in the same way as SK-N-AS and SK-N-BE.

Animals

C57BL/6J female mice (Clea Japan, Tokyo, Japan) were dissected under pentobarbital anesthesia (i.p.), and the abdominal vessels were cut to drain the blood. Tissues were removed and whole cell extracts or total RNA was prepared. The handling and killing of all animals used in this study were in accordance with the national prescribed guidelines, and ethical approval for the studies was granted by the Animal Experiment Committee of Kyushu University (Fukuoka, Japan).

Nucleic Acids

Oligo-DNAs (see Supplemental Materials) and nucleotide-immobilized Sepharoses were purchased from Sigma-Aldrich Japan (Tokyo, Japan) and Jena Bioscience (Jena, Germany), respectively.

Identification of 8-Oxo-GTP-Binding Protein

8-Oxo-GTP-binding proteins were purified from thymocyte extracts prepared from 5-week-old mice by a pull-down method using γ-aminooctyl-8-oxo-GTP-Sepharose and were subjected to liquid chromatography–tandem mass spectrometry (LC–MS/MS) as previously reported (Nonaka et al. 2009).

Cloning of PRUNE2 cDNA and Construction of Plasmids

Total RNA was prepared from HeLa MR using ISOGEN (Nippon Gene, Tokyo, Japan). First-strand cDNAs were synthesized using PrimeScript® Reverse Transcriptase (Takara, Kyoto, Japan) with an oligo(dT) primer. *PRUNE2* cDNA was amplified by nested PCR using PrimeStar® GXL DNA Polymerase (Takara), as described below. Forty cycles of first PCR and 15 cycles of second PCR were performed using 5hPr2LAnest/3hPr2LAnest and 5hPr2LA-*Sal*I/3hPr2LA-*Sac*II as primer sets, respectively. The second PCR product was inserted into the *Sal*I/*Sac*II site of pIRES2-EGFP (Clontech, Palo Alto, CA, USA) to generate pIRES2-EGFP:PRUNE2. Sequence of the *PRUNE2* cDNA was confirmed with the sequencing primers (see Supplemental Materials).

To express the N-terminal region of PRUNE2 (hPr2N, 1–359 aa), we performed PCR using pIRES2-EGFP:PRUNE2 as a template and hPr2-*Nde*IATG/3hPr2Ab-STOP*Xho*I-NH as a primer set. The *Nde*I/*Xho*I fragment was inserted into the *Nde*I/*Xho*I site of pET28a(+) (Merck, Darmstadt, Germany), thus constructing pET28a(+):His-hPr2N encoding N-terminal His-tagged hPr2N.

Preparation of Polyclonal Antibodies Against PRUNE2 (Anti-hPr2N Ig)

Rabbit polyclonal antibodies against the hPr2N were prepared and purified using pET28a(+):His-hPr2N as previously described (Nakabeppu and Nathans 1991) and were designated anti-hPr2N immunoglobulin (Ig).

Western Blot Analysis

Western blot analysis was performed using 1 μg/ml of anti-hPr2N Ig, as previously described (Tsuchimoto et al. 2001).

Immunoprecipitation

HeLa MR and HEK293T cells were suspended in radioimmunoprecipitation assay (RIPA) lysis buffer (50 mM

Tris–Cl pH 8.0, 150 mM NaCl, 1% Nonidet P-40 [NP-40], 0.5% deoxycholic acid, 0.1% sodium dodecyl sulfate) and incubated for 10 min at 4°C. Each supernatant was collected as a RIPA soluble fraction after centrifugation at 100,000×*g* for 15 min at 4°C. KNS81 cells were suspended in hypotonic NP-40 lysis buffer (10 mM Tris–Cl pH 7.4, 10 mM NaCl, 5 mM $MgCl_2$, 0.5% NP-40, 1× protease inhibitor cocktail [Nacalai Tesque, Kyoto, Japan]) and incubated for 10 min at 4°C. The supernatant was collected as an NP-40 cytoplasm fraction after centrifugation at 2,000×*g* for 20 min at 4°C. Immunoprecipitation from the RIPA soluble fraction or NP-40 cytoplasm fraction was performed with anti-hPr2N Ig or control normal rabbit Ig (Sigma-Aldrich, St Louis, MO, USA) as previously described (Torisu et al. 2005). Immunoprecipitation samples were subjected to SDS-PAGE, Western blot, or LC–MS/MS.

Nucleotide Binding Assay

Cytoplasmic fractions were prepared from KNS81, SK-N-AS, SK-N-BE, and NB-1 cells (as described above) in NP-40 lysis buffer with 5 mM 2-mercaptoethanol and mixed with 60 μl of 50% equilibrated γ-aminooctyl-GTP-Sepharose, γ-aminooctyl-8-oxo-GTP-Sepharose, 2′/3′-O-(2-aminoethylcarbamoyl)-GTP-Sepharose, 2′/3′-O-(2-aminoethyl-carbamoyl)-8-oxo-GTP-Sepharose, or carrier-Sepharose. After rotating the mixture for 15 min, the Sepharoses were washed with lysis buffer three times. Bound proteins were subjected to Western blot analysis.

Knockdown of PRUNE2 Expression

Small interfering RNAs (siRNAs) against human *PRUNE2* (#s46086, #s228804) and control siRNA (*Silencer*® Select Negative Control #1) were purchased from Applied Biosystems (Foster City, CA, USA) (see Supplemental Materials) and introduced into cells using a Microporator-Mini (Digital Bio Technology, Seoul, South Korea). The cells were collected at 48 or 72 h after the introduction to extract total RNA or protein.

Quantitative Real Time RT-PCR Analysis

Total RNAs were prepared using ISOGEN, except total RNAs from human tissues, which were purchased from Clontech. cDNA synthesis was performed using random hexamer primers and PrimeScript® Reverse Transcriptase for mouse RNAs or using random hexamer primers and High Capacity cDNA Reverse Transcription kit (Applied Biosystems) for human RNAs. Quantitative real time RT-PCR was performed as previously described (Nonaka et al. 2009). Serially diluted cDNA was used to obtain a standard curve for each transcript. The levels of mRNA were normalized to that of 18S ribosomal RNA in each sample.

Immunohistochemistry

Human dorsal root ganglion (DRG) postmortem tissue from a 54-year-old female was provided by Dr. Toru Iwaki from the Department of Neuropathology, Neurological Institute, Graduate School of Medical Sciences, Kyushu University. Kyushu University approved this study, participants provided written informed consent, and procedures followed were in accordance with national guidelines. The tissues were fixed in 10% formalin and cryoprotected in 20% and 30% sucrose and were frozen at −80°C. Serial sections (6 μm thickness) were cut on a cryostat and treated with acetone at 4°C for 5 min. Immunostaining of the sections and detection of signals were performed with anti-hPr2N Ig at 10 μg/ml or mouse anti-Schwann monoclonal Ig (Schwann/2E, COSMO BIO, Tokyo, Japan) at a 1:1,000 dilution as described (Kajitani et al. 2006). The slides were subjected to counterstaining by hematoxylin.

Results

Cloning of Full-Length cDNAs and Structural Analysis of the PRUNE2 Gene

Using γ-aminooctyl-8-oxo-GTP-Sepharose, we purified 8-oxo-GTP-binding proteins from a mouse thymocyte extract, and LC–MS/MS analysis revealed that the bound fraction contained a peptide (MEEFLQR, MASCOT ion score=44) corresponding to the N-terminal of hypothetical PRUNE2 protein (NP_851993). The human *PRUNE2* gene is expected to be transcribed to a single mRNA (NM_015225.2) covering two genes previously identified as *C9orf65* and *BMCC1* (Machida et al. 2006; Price et al. 2007), and a large protein composed of 3,088 amino acid residues is expected to be translated. We isolated cDNA clones [DDBJ: AB535152] carrying the full-length PRUNE2 coding sequence amplified by nested RT-PCR of total RNA from HeLa MR cells. Sequence comparison between the isolated cDNA and human genomic DNA using the BLAST program (Altschul et al. 1990) revealed that *PRUNE2* is located on chromosome 9 (9q21.2), spans about 295 kbp, and consists of 18 exons (Fig. 1a). The 5′ region from exon 1 to exon 6 of *PRUNE2* corresponds to *C9orf65* whose transcript terminates in intron 6 of *PRUNE2*, while its 3′ region from exon 8 to exon 18 corresponds to *BMCC1*, whose transcript contains an extra exon between exon 17 and 18 of *PRUNE2*. Therefore, we demonstrated that these two cancer-related genes are transcribed as a single mRNA for PRUNE2 protein. The isolated *PRUNE2* cDNA encoded a protein

consisting of 3,062 amino acid residues (Fig. 2), which is slightly different from the sequence (NP_056040) in the database and may result from altered splicing. Sequence alignment revealed that the N-terminal 617 amino acid sequence of PRUNE2 shares homology with PRUNE (Fig. 1b, c), while the C-terminal region starting at the 360th methionine residue corresponds to BMCC1, which contains a coiled-coil sequence, proline-rich region, P-loop, and BNIP2 homology C-terminal region containing a BCH domain (Fig. 1b).

PRUNE2 mRNA in Cell Lines Derived from Human Tumors

We examined the expression levels of *PRUNE2* mRNA in human cell lines and whole brain by quantitative real time RT-PCR using the primer set, RT900 (Fig. 3a). As shown in Fig. 3b, relatively higher levels of *PRUNE2* mRNA were detected in KNS81 derived from glioblastoma than in HeLa MR derived from cervical adenocarcinoma and whose levels were lower than that in normal adult brain. On the other hand, the expression of *PRUNE2* mRNA was undetectable in SH-SY5Y, a cell line derived from an unfavorable type of neuroblastoma from a bone metastasis in a 4-year-old patient (Biedler et al. 1973).

We then examined the effects of two siRNAs for *PRUNE2* on its expression in KNS81 cells. The target sites of the two siRNAs (#01 and #04) were placed in exon 2 and exon 6 of *PRUNE2* mRNA, and the four real time PCR primer sets, hPr2RT, RT900, RT6000, and RT7500, were placed in exon 1/2 junction, exon 7, exon 8, and exon 8/9 junction, respectively (Fig. 3a). First, we introduced siRNA #01 (exon 2) or #04 (exon 6) to KNS81 cells and estimated the *PRUNE2* mRNA levels at 48 h after the introduction by quantitative real time RT-PCR using the primer set, hPr2RT (exon 1/2). siRNA #01 and #04 decreased the *PRUNE2* mRNA to levels less than 50% or 20% of that seen in the cells treated with control siRNA, respectively (Fig. 3c).

To examine the effects of *PRUNE2* siRNA #01 (exon 2) on the transcript harboring different downstream sequences from exons 7 to 9, we compared the levels of transcripts amplified by the three primer sets, RT900 (exon 7), RT6000 (exon 8), and RT7500 (exon 8/9), in HeLa MR cells. In the cells treated with siRNA #01, the levels of transcripts amplified by the three sets of primers were similarly suppressed at approximately 45% of that of control cells (Fig. 3d). These results also suggest that *C9orf65* and *BMCC1* are transcribed as a single transcript of *PRUNE2* (Fig. 1a).

Identification of Endogenous PRUNE2 Protein

Since there was no experimental evidence for the presence of human PRUNE2 protein, we prepared anti-hPr2N Ig against the N-terminal region of PRUNE2 lacking the BMCC1 sequence and applied the antibodies to immunoprecipitation and Western blotting analysis of HeLa MR cell extract. A major immunoreactive band that migrated significantly more slowly than the 250-kDa marker protein was detected in the sample precipitated by anti-hPr2N Ig, but not in samples using control Ig (the arrowhead in Fig. 4a). In SDS-PAGE analysis, the migration of the recombinant full-length PRUNE2 expressed in HEK293T cells and the band detected in HeLa MR cells was indistinguishable. These results indicate that the immunoreactive band in HeLa MR cells represents the endogenous full-length PRUNE2 protein.

We then performed immunoprecipitation from a KNS81 cytoplasmic extract and separated the immunoprecipitated proteins by SDS-PAGE (Fig. 4b, left). Each lane of the gel was collected, separated into ten pieces, treated with trypsin G, and subjected to LC–MS/MS analysis. Two peptides derived from the N-terminal region and 11 peptides derived from the C-terminal BMCC1 region of PRUNE2 were detected in the gel region corresponding to proteins greater than 250-kDa from the sample precipitated by anti-hPr2N, but not by control Ig (Fig. 2). The C-terminal BMCC1 region did not exhibit any homology to the amino acid sequence of the antigen, hPr2N, indicating that the precipitated protein carries both the N-terminus and C-terminus of PRUNE2. To elucidate the physiological role of PRUNE2, we applied LC–MS/MS analysis to immunoprecipitates from KNS81 cell extracts and identified 20 proteins as candidates for PRUNE2-associating proteins (Table 1).

We further examined the effects of the knockdown of *PRUNE2* expression in KNS81 cells and found that siRNA #04 significantly reduced the level of the largest anti-hPr2N-reactive band compared with that using the control siRNA (Fig. 4b, right). These results provide additional evidence indicating that the largest anti-hPr2N-reactive band

Fig. 1 Structure of the *PRUNE2* gene and its translation product. **a** Genomic structure of the *PRUNE2* gene. *PRUNE2* consists of 18 exons. The first five exons correspond to those of *C9orf65* and a part of intron 6 is transcribed as exon 6 of *C9orf65* (*in red*) (*single asterisk*). The last 11 exons correspond to most of the *BMCC1* sequence. *BMCC1* is translated from a methionine codon in exon 8 of *PRUNE2* (*two asterisks*), which corresponds to the 360th residue of PRUNE2. Exon 13 of *PRUNE2* is spliced out (*three asterisks*) and an additional exon is inserted between exon 17 and exon 18 of *PRUNE2* for *BMCC1* mRNA (*in red*) (*four asterisks*). **b** Structure of the PRUNE2 protein. The hPr2N region, the PRUNE homology domain, the BMCC1 region, the coiled-coil sequence, proline-rich sequence, P-loop, BNIP2 homology C-terminal region, and BCH domain are shown. **c** Homology between PRUNE and PRUNE2. The N-terminal 617 amino acids of PRUNE2 and the N-terminal 416 amino acids of PRUNE were aligned by ClustalX software version 2.0 (Larkin et al. 2007). Identical residues are *shaded black*

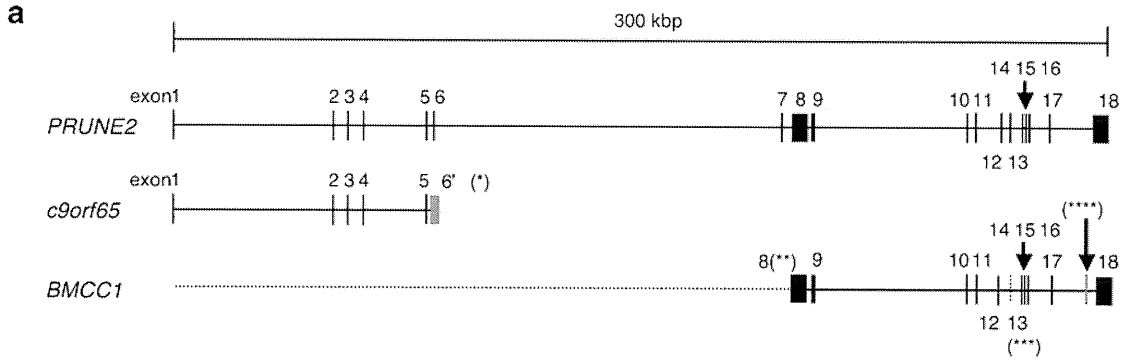

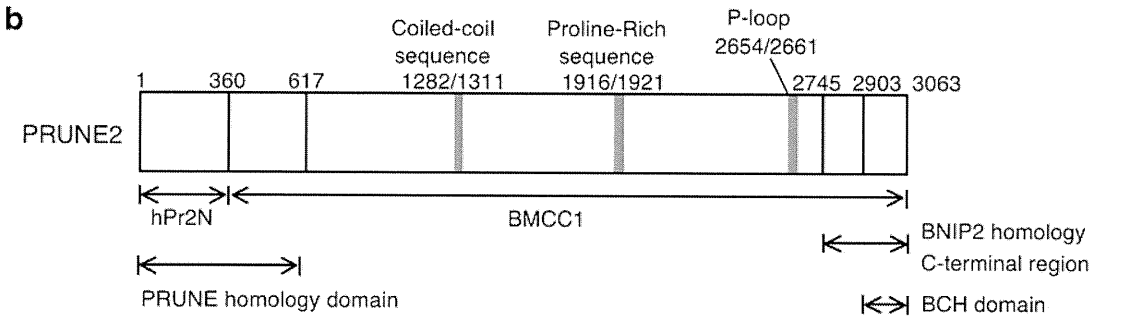

c

```
PRUNE (1-416)     1 MEDYLQGCRAAIQESR---PLHVVLGNEACDLDSTVSALALAFYLAKTTEAEEVFVPVLN  57
PRUNE2 (1-617)    1 MEEFLQRAKSKLNRSKRLEKVHVVIGPKSCDLDSLISTFTYAYFLDKVSPPGVLCLPVLN  60

PRUNE (1-416)    58 IKRSELPLRGDIVFFLQKVHIPESILIFRDEIDLHALYQAGQLTLILVDHHILSKSDTAL  117
PRUNE2 (1-617)   61 IPRTEFNYFTETRFILEELNISESFHIFRDEINLHQLNDEGKLSITLVGSSVLASEDKTL  120

PRUNE (1-416)   118 EEAVAEVLDHRPIEPKHCPPCHVSVELVGSCATLVTERILQGAPEILDRQTAALLHGTII  177
PRUNE2 (1-617)  121 ESAVVKVIN--PVE------QSDANVEFRESSSSLVLKEILQEAPELITEQLAHRLRGSIL  173

PRUNE (1-416)   178 LDCVNMDLKIGKATPKDSKYVEKLEALFPDLPKRNDIFDSLQKAKFDVSGLTTEQMLRKD  237
PRUNE2 (1-617)  174 FKWMTMES--EKISEKQEEILSILEEKFPNLPPREDIINVLQETQFSAQGLSIEQTMLKD  231

PRUNE (1-416)   238 QKTIYRQGVKVAISAIYMDLEAFLQRSNLLADLHAFCQAHSYDVLVAMTIFFNTHNEPVR  297
PRUNE2 (1-617)  232 LKELSDGEIKVAISTVSMNLENCLFHSNITSDIKAFTDKFGFDVLILFSSYLSEEQQPRR  291

PRUNE (1-416)   298 QLAIFCPHVALQTTICEVLERSHSPPIKLTPASSTHPNLHAVLQGNTQVSRKKLLPLLQE  357
PRUNE2 (1-617)  292 QIAVYSENMELCSQICCELEECQNDCLELEFDCGCDEILVYQQEDPSVTCDQVVLVVKE  351

PRUNE (1-416)   358 ALS----------AYFDSMKIPSGQ----------PETAD  377
PRUNE2 (1-617)  352 VINRRCPEMVSNSRTSSTEAVAGSAPLSQGSSGIMELYGSDIEPQPSSVNFIENPPDLND  411

PRUNE (1-416)   378 VSREQVDKELDRAS----------  391
PRUNE2 (1-617)  412 SNQAQVDANVDLVSPDSGLATIRSSRSSKESSVFLSDDSPVGEGAGPHHTLLPGLDSYSP  471

PRUNE (1-416)   391 ----------  391
PRUNE2 (1-617)  472 IPEGAVAEEHAWSGEHGEHFDLFNFDPAPMASGQSQQSSHSADYSPADDFFPNSDLSEGQ  531

PRUNE (1-416)   392 ----------NSLISCLSQD----------EEDPP----------  406
PRUNE2 (1-617)  532 LPAGPEGLDGMGTNMSNYSSSSLLSCAGKDSLVEHDEEFVQRQDSPRDNSERNLSLTDFV  591

PRUNE (1-416)   407 ----------LPPTPMNSLV  416
PRUNE2 (1-617)  592 GDESPSPERLKNTGKRIPPTPMNSLV  617
```

corresponds to the endogenous full-length PRUNE2 protein. Therefore, we conclude that an endogenous full-length PRUNE2 protein harboring the PRUNE homology domain and BMCC1 sequence was identified in human cells.

To confirm whether full-length human PRUNE2 interacts with nucleotides such as 8-oxo-GTP, we performed a pull-down assay from the extract of KNS81 cells using GTP-Sepharoses, 8-oxo-GTP-Sepharoses, and carrier-

MEEFLQRAKSKLNRSKRLEKVHVVIGPKSCDLDSLISTFTYAYFLDKVSPPGVLCLPVLNIPRTEFN
YFTETRFILEELNISESFHIFRDEINLHQLNDEGKLSITLVGSSVLASEDKTLESAVVKVINPVEQS
DANVEFRESSSSLVLKEILQEAPELITEQLAHRLRGSILFKWMTMESEKISEKQEEILSILEEKFPN
LPPREDIINVLQETQFSAQGLSIEQTMLKDLKELSDGEIKVAISTVSMNLENCLFHSNITSDLKAFT
DKFGFDVLILFSSYLSEEQQPRRQIAVYSENMELCSQICCELEECQNPCLELEPFDCGCDEILVYQQ
EDPSVTCDQVVLVVKEVINRRCPEMVSNSRTSSTEAVAGSAPLSQGSSGIMELYGSDIEPQPSSVNF
IENPPDLNDSNQAQVDANVDLVSPDSGLATIRSSRSSKESSVFLSDDSPVGEGAGPHHTLLPGLDSY
SPIPEGAVAEEHAWSGEHGEHFDLFNFDPAPMASGQSQQSSHSADYSPADDFFPNSDLSEGQLPAGP
EGLDGMGTNMSNYSSSSLLSGAGKDSLVEHDEEFVQRQDSPRDNSERNLSLTDFVGDESPSPERLKN
TGKRIPPTPMNSLVESSPSTEEPASLYTEDMTQKATDTGHMGPPQTHARCSSWWGGLEIDSKNIADA
WSSSEQESVFQSPESWKEHKPSSIDRRASDSVFQPKSLEFTKSGPWESEFGQPELGSNDIQDKNEES
LPFQNLPMEKSPLPNTSPQGTNHLIEDFASLWHSGRSPTAMPEPWGNPTDDGEPAAVAPFPAWSAFG
KEDHDEALKNTWDLHPTSSKTPSVRDPNEWAMAKSGFAFSSSELLDNSPSEINNEAAPEIWGKKNND
SRDHIFAPGNPSSDLDHTWTNSKPPKEDQNGLVDPKTRGKVYEKVDSWNLFEENMKKGGSDVLVPWE
DSFLSYKCSDYSASNLGEDSVPSPLDTNYSTSDSYTSPTFAGDEKETEHKPFAKEEGFESKDGNSMA
EETDIPPQSLQQSLQQSSRNRISSGPGNLDMWASPHTDNSSEINTTHNLDENELKTEHTDGKNISME
DDVGESSQSSYDDPSMMQLYNETNRQLTLLHSSTNSRQTAPDSLDLWNRVILEDTQSTATISDMDND
LDWDDCSGGAAIPSDGQTEGYMAEGSEPETRFTVRQLEPWGLEYQEANQVDWELPASDEHTKDSAPS
EHHTLNEKSGQLIANSIWDSVMRDKDMSSFMLPGSSHITDSEQRELPPEIPSHSANVKDTHSPDAPA
ASGTSESEALISHLDKQDTERETLQSDAASLATRLENPGYFPHPDPWKGHGDGQSESEKEAQGATDR
GHLDEEEVIASGVENASGISEKGQSDQELSSLVASEHQEICIKSGKISSLAVTFSPQTEEPEEVLEY
EEGSYNLDSRDVQTGMSADNLQPKDTHEKHLMSQRNSGETTETSDGMNFTKYVSVPEKDLEKTEECN
FLEPENVGGGPPHRVPRSLDFGDVPIDSDVHVSSTRSEITKNLDVKGSENSLPGAGSSGNFDRDTIS
SEYTHSSASSPELNDSSVALSSWGQQPSSGYQEENQGNWSEQNHQESELITTDGQVEIVTKVKDLEK
NRINEFEKSFDRKTPTFLEIWNDSVDGDSFSSLSSPETGKYSEHSGTHQESNLIASYQEKNEHDISA
TVQPEDARVISTSSGSDDDSVGGEESIEEEIQVANCNVAEDESRAWDSLNESNKFLVTADPKSENIY
DYLDSSEPAENENKSNPFCDNQQSSPDPWTFSPLTETEMQITAVEKEKRSSPETGTTGDVAWQISPK
ASFPKNEDNSQLEMLGFSADSTEWWKASPQEGRLIESPFERELSDSSGVLEINSSVHQNASPWGVPV
QGDIEPVETHYTNPFSDNHQSPFLEGNGKNSHEQLWNIQPRQPDPDADKFSQLVKLDQIKEKDSREQ
TFVSAAGDELTPETPTQEQCQDTMLPVCDHPDAAFTHAEENSCVTSNVSTNEGQETNQWEQEKSYLG
EMTNSSIATENFPAVSSPTQLIMKPGSEWDGSTPSEDSRGTFVPDILHGNFQEGGQLASAAPDLWID
AKKPFSLKADGENPDILTHCEHDSNSQASDSPDICHDSEAKQETEKHLSACMGPEVESSELCLTEPE
IDEEPIYEPGREFVPSNAELDSENATVLPPIGYQADIKGSSQPTSHKGSPEPSEINGDNSTGLQVSE
KGASPDMAPILEPVDRRIPRIENVATSIFVTHQEPTPEGDGSWISDSFSPESQPGARALFDGDPHLS
TENPALVPDALLASDTCLDISEAAFDHSFSDASGLNTSTGTIDDMSKLTLSEGHPETPVDGDLGKQD
ICSSEASWGDFEYDVMGQNIDEDLLREPEHFLYGGDPPLEEDSLKQSLAPYTPPFDLSYLTEPAQSA
ETIEEAGSPEDESLGCRAAEIVLSALPDRRSEGNQAETKNRLPGSQLAVLHIREDPESVYLPVGAGS
NILSPSNVDWEVETDNSDLPAGGDIGPPNGASKEIPELEEEKTIPTKEPEQIKSEYKEERCTEKNED
RHALHMDYILVNREENSHSKPETCEERESIAELELYVGSKETGLQGTQLASFPDTCQPASLNERKGL
SAEKMSSKGDTRSSFESPAQDQSWMFLGHSEVGDPSLDARDSGPGWSGKTVEPFSELGLGEGPQLQI
LEEMKPLESLALEEASGPVSQSQKSKSRGRAGPDAVTHDNEWEMLSPQPVQKNMIPDTEMEEETEFL
ELGTRISRPNGLLSEDVGMDIPFEEGVLSPSAADMRPEPPNSLDLNDTHPRRIKLTAPNINLSLDQS
EGSILSDDNLDSPDEIDINVDELDTPDEADSFEYTGHEDPTANKDSGQESESIPEYTAEEEREDNRL
WRTVVIGEQEQRIDMKVIEPYRRVISHGGDSGYYGDGLNAIIVFAACFLPDSSRADYHYVMENLFLY
VISTLELMVAEDYMIVYLNGATPRRRMPGLGWMKKCYQMIDRRLRKNLKSFIIVHPSWFIRTILAVT
RPFISSKFSSKIKYVNSLSELSGLIPMDCIHIPESIINIDLKLKEKP

◀**Fig. 2** Amino acid sequence of PRUNE2. The isolated *PRUNE2* cDNA encodes a protein consisting of 3,062 amino acids. The hPr2N region used for rabbit immunization is *boxed*. The other region corresponds to BMCC1. Among the 13 peptides detected by LC–MS/MS analysis of the sample precipitated with anti-hPr2N Ig, the five peptides with high MASCOT ion scores (>50) and the other eight peptides with low scores (<50) are shown *in red* and *blue*, respectively

Sepharose. By Western blot analysis using anti-hPr2N Ig, an immunoreactive band corresponding to the full-length PRUNE2 was detected in the 8-oxo-GTP-Sepharoses and GTP-Sepharoses-bound samples, but not in the carrier-Sepharose-bound sample (Fig. 4c). We also examined the expression levels of PRUNE2 in five different cell lines derived from neuroblastoma cells. In contrast to KNS81 and HeLa MR, Western blot with anti-Pr2N Ig revealed that there are more than ten immunoreactive bands with molecular weights ranging from 50 to more than 250 kDa, among which a band with the lowest mobility in each lane co-migrates with the full-length PRUNE2 detected in KNS81 (Fig. 4d). We prepared extracts from the three cell lines, SK-N-AS, SK-N-BE, and NB-1, which exhibited relatively high levels of the full-length PRUNE2, although it was not a major form. We found that a small amount of full-length PRUNE2 was recovered in an extract prepared with NP-40 lysis buffer from NB-1 cells only (Fig. 4e, left), suggesting that most of the full-length PRUNE2 might be lost by degradation or precipitation during extraction. We then performed pull-down assays with extracts prepared from the three cell lines using ribose linked GTP-Sepharose, 8-oxo-GTP-Sepharose, and carrier-Sepharose. Only in the sample from NB-1 cells was a faint signal corresponding to the full-length PRUNE2 observed to bind to GTP-Sepharose and 8-oxo-GTP-Sepharose, but not to carrier-Sepharose (Fig. 4e, right). Moreover, an intense signal corresponding to a 120-kDa polypeptide and less intense signals corresponding to polypeptides with lower molecular weights were specifically detected in GTP-Sepharose-bound fractions prepared from all three cell lines. Among them only a 50-kDa band was found to bind to 8-oxo-GTP (Fig. 4e, right).

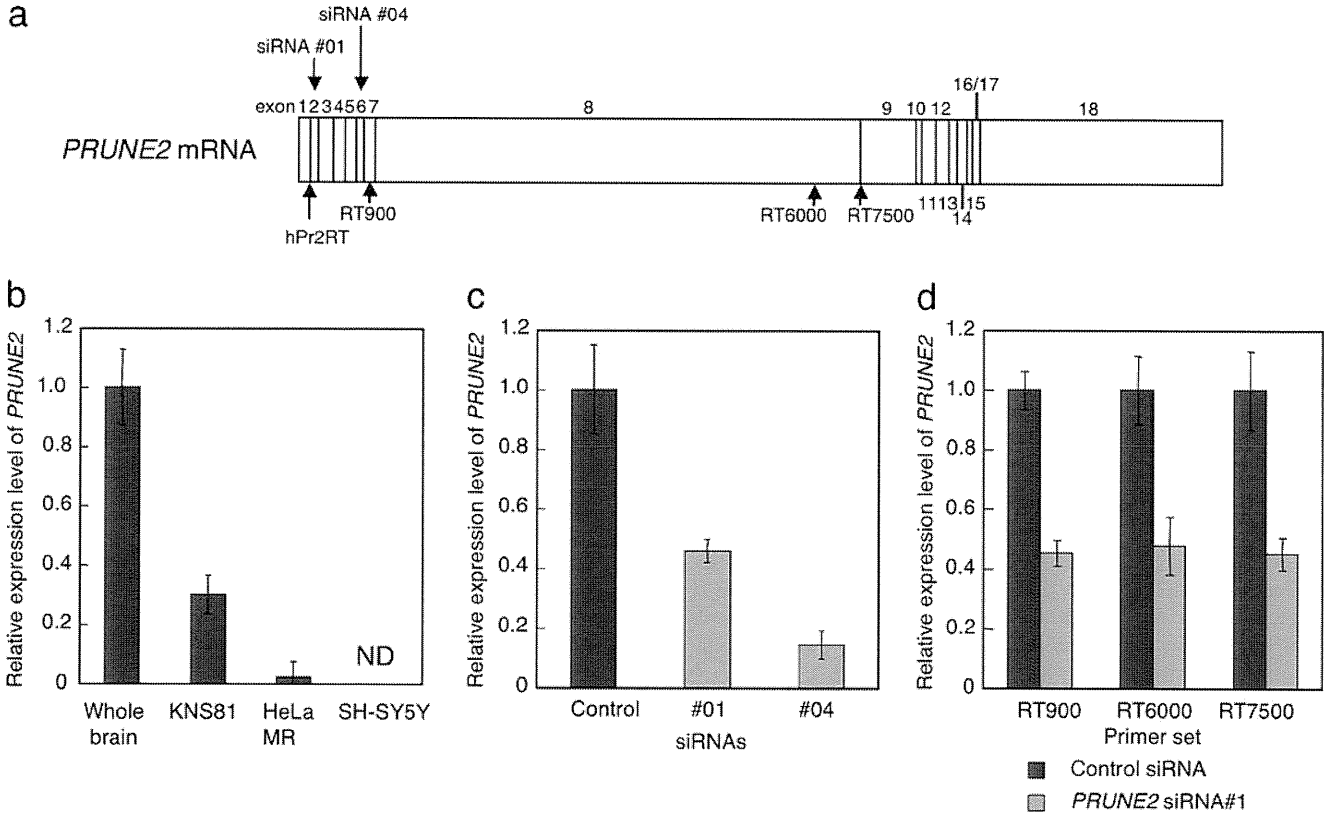

Fig. 3 *PRUNE2* mRNA in human tumor cell lines. **a** The target sites of the two *PRUNE2* siRNAs (#01 and #04) and the four primer sets for real time PCR, hPr2RT, RT900, RT6000, and RT7500. **b** *PRUNE2* mRNA levels in human cancer cell lines analyzed by quantitative real time RT-PCR using the primer set, RT900. **c** *PRUNE2* mRNA levels in KNS81 after siRNA treatment. *PRUNE2* mRNA was quantified by real time quantitative RT-PCR using the primer set, hPr2RT. **d** Quantitative real time RT-PCR of *PRUNE2* mRNA using three primer sets, RT900, RT6000, and RT7500, after introduction of siRNA #01 to HeLa MR cells. The levels of relative expression are expressed as the mean ± SD of three measurements